Title

Macrophage COX2 Mediates Efferocytosis, Resolution Reprogramming, and Intestinal Epithelial Repair

Journal

Cellular and Molecular Gastroenterology and Hepatology, 13(4)

ISSN

2352-345X

Authors

Meriwether, David
Jones, Anthony E
Ashby, Julianne W
et al.

Publication Date

2022

DOI

10.1016/j.jcmgh.2022.01.002

cmgh
CELLULAR AND MOLECULAR GASTROENTEROLOGY AND HEPATOLOGY

ORIGINAL RESEARCH

Macrophage COX2 Mediates Efferocytosis, Resolution Reprogramming, and Intestinal Epithelial Repair

David Meriwether,[1,2] Anthony E. Jones,[3] Julianne W. Ashby,[2] R. Sergio Solorzano-Vargas,[4] Nasrin Dorreh,[2] Shoreh Noori,[2] Victor Grijalva,[2] Andréa B. Ball,[3] Margarita Semis,[2] Ajit S. Divakaruni,[3] Julia J. Mack,[2] Harvey R. Herschman,[3] Martin G. Martin,[4] Alan M. Fogelman,[2] and Srinivasa T. Reddy[2,3]

[1]Division of Digestive Diseases, Department of Medicine, David Geffen School of Medicine, University of California, Los Angeles, Los Angeles, California; [2]Division of Cardiology, Department of Medicine, David Geffen School of Medicine, University of California, Los Angeles, Los Angeles, California; [3]Department of Medical and Molecular Pharmacology, University of California, Los Angeles, Los Angeles, California; and [4]Division of Gastroenterology, Department of Pediatrics, David Geffen School of Medicine, University of California, Los Angeles, Los Angeles, California

SUMMARY

Efferocytosis of apoptotic neutrophils by macrophages anchors the resolution of intestinal inflammation and is implicated in the pathogenesis of inflammatory bowel disease. We demonstrate that macrophage cyclooxygenase 2 potentiates efferocytosis capacity and facilitates efferocytosis-dependent macrophage reprogramming and intestinal epithelial repair.

BACKGROUND AND AIMS: Phagocytosis (efferocytosis) of apoptotic neutrophils by macrophages anchors the resolution of intestinal inflammation. Efferocytosis prevents secondary necrosis and inhibits further inflammation, and also reprograms macrophages to facilitate tissue repair and promote resolution function. Macrophage efferocytosis and efferocytosis-dependent reprogramming are implicated in the pathogenesis of inflammatory bowel disease. We previously reported that absence of macrophage cyclooxygenase 2 (COX2) exacerbates inflammatory bowel disease–like intestinal inflammation. To elucidate the underlying pathogenic mechanism, we investigated here whether COX2 mediates macrophage efferocytosis and efferocytosis-dependent reprogramming, including intestinal epithelial repair capacity.

METHODS: Using apoptotic neutrophils and synthetic apoptotic targets, we determined the effects of macrophage specific *Cox2* knockout and pharmacological COX2 inhibition on the efferocytosis capacity of mouse primary macrophages. COX2-mediated efferocytosis-dependent eicosanoid lipidomics was determined by liquid chromatography tandem mass spectrometry. Small intestinal epithelial organoids were employed to assay the effects of COX2 on efferocytosis-dependent intestinal epithelial repair.

RESULTS: Loss of COX2 impaired efferocytosis in mouse primary macrophages, in part, by affecting the binding capacity of macrophages for apoptotic cells. This effect was comparable to that of high-dose lipopolysaccharide and was accompanied by both dysregulation of macrophage polarization and the inhibited expression of genes involved in apoptotic cell binding. COX2 modulated the production of efferocytosis-dependent lipid inflammatory mediators that include the eicosanoids prostaglandin I2, prostaglandin E2, lipoxin A4, and 15d-PGJ2; and further affected secondary efferocytosis. Finally, macrophage efferocytosis induced, in a macrophage COX2–dependent manner, a tissue restitution and repair phenotype in intestinal epithelial organoids.

CONCLUSIONS: Macrophage COX2 potentiates efferocytosis capacity and efferocytosis-dependent reprogramming, facilitating macrophage intestinal epithelial repair capacity. *(Cell Mol Gastroenterol Hepatol 2022;13:1095–1120; https://doi.org/10.1016/j.jcmgh.2022.01.002)*

Keywords: Macrophage; Inflammation Resolution; Inflammatory Bowel Disease; Lipidomics; Eicosanoids.

Inflammatory bowel disease (IBD)—including both ulcerative colitis and Crohn's disease (CD)—is a chronic and relapsing inflammatory disorder of the intestinal tract. IBD includes a dysregulated mucosal immune response to commensal gut microbiota, often brought about by environmental triggers in genetically susceptible individuals.[1]

Abbreviations used in this paper: **1°, primary; 2°, secondary; AA, arachidonic acid; apMPRO, apoptotic MPRO; AnV, annexin V; BL6, C57BL/6 mice; BMDM, bone marrow–derived macrophage; BP, barrier permeability; BSA, bovine serum albumin; CCHF, cholate-containing high fat diet; CD, Crohn's disease; CM, conditioned media; COX2, cyclooxygenase 2; COX2i, COX2 pharmacologic inhibition; CSF, colony-stimulating factor; FBS, fetal bovine serum; FLOX, *Cox2* floxed; HGF, hepatocyte growth factor; IBD, inflammatory bowel disease; IL, interleukin; KO, total knockout; LC-MS/MS, liquid chromatography tandem mass spectrometry; LP, lamina propria; LPS, lipopolysaccharide; LXA4, lipoxin A4; MKO, myeloid-specific knockout; MRM, multiple reaction monitoring; NT, no treatment; PBS, phosphate-buffered saline; PC, phosphatidylcholine; PE, phosphatidylethanolamine; PG, prostaglandin; PM, peritoneal macrophage; PS, phosphatidylserine; qPCR, quantitative polymerase chain reaction; TLR, Toll-like receptor; TNFα, tumor necrosis factor α; WAE, wound-associated epithelium; WT, wild-type.**

Most current article

2352-345X
https://doi.org/10.1016/j.jcmgh.2022.01.002

Over 200 genetic susceptibility or risk loci, including cyclooxygenase 2 (*COX2*) (also known as *PTGS2*), have been identified for IBD.[2] Pathway analysis of prognosis-associated SNPs has implicated regulation of innate immune responses and mononuclear phagocytes in CD prognosis.[3]

COX2 is an inducible enzyme responsible for the rate-limiting step in the conversion of arachidonic acid to prostanoids.[4] While COX2 is commonly thought to be proinflammatory, we recently reported that myeloid-specific knockout (MKO) of *Cox2* causes mice to develop Toll-like receptor (TLR)–dependent CD-like inflammation when intestinal barrier function is compromised by a cholate-containing high-fat (CCHF) diet.[5] Macrophage COX2 thus appears to provide an inhibitory check on TLR-dependent intestinal inflammation. In part, this check may be anti-inflammatory. Consistent with prior reports,[6–8] we observed an increased LPS-dependent expression of inflammatory cytokines in *Cox2* MKO macrophages.[5] However, macrophage COX2 may also modulate inflammation resolution. Lipoxin A4 (LXA4) is a potent lipid inflammatory mediator that can be synthesized from arachidonic acid via macrophage COX2-dependent production of 15HETE.[9] LXA4 is broadly anti-inflammatory, but it can also increase the inflammation macrophage resolving capacity.[10] We observed that *Cox2* MKO reduced the level of LXA4 in intestinal inflammatory lesions of CCHF-fed mice and that administration of a stable LXA4 analog rescued disease. We speculated that absence of COX2 compromised the resolving capacity of macrophages, and that this dysfunction contributed to the intestinal pathology of our IBD model.[5]

Physiological inflammation is self-limiting, and the resolution of inflammation is an active and coordinated process.[11] Acute intestinal inflammation starts upon detection of pathogen or damage-associated molecular patterns, leading initially to a coordinated trafficking of neutrophils and inflammatory monocytes into the lamina propria (LP). The resolution process begins with neutrophil apoptosis, but macrophages play at least 2 roles whose impairment could lead to chronic intestinal inflammation. First, clearance of apoptotic neutrophils is necessary to prevent secondary necrosis and further inflammation.[12] Macrophages first find and then phagocytose apoptotic neutrophils in a process known as efferocytosis.[13] Within the LP, the macrophage population of the inflammatory microenvironment must thus be capable of naïve or primary efferocytosis—of initiating efferocytosis with respect to an increasingly apoptotic neutrophil population.[14] Second, efferocytosis of apoptotic cells reprograms macrophages from an inflammatory to an anti-inflammatory, resolving, and tissue repair phenotype somewhat akin to that of mature resident macrophages.[14,15] This reprogramming shifts the inflammatory distribution of cytokines, suppressing expression of interleukin (IL)-1β and IL-12 while increasing both IL-10 and transforming growth factor β.[16] This reprograming includes upregulation of genes involved in efferocytosis itself,[13] thereby increasing secondary efferocytosis capacity. Finally, the initial efferocytosis increases production of trophic and repair factors like annexin A1 and extracellular vesicle–packaged WNTs that are important for re-establishing the epithelial barrier following disruption of the intestinal epithelium.[14] Thus, inflammatory, immature LP macrophages must successfully reprogram following naïve efferocytosis to suppress neutrophil chemotaxis and Th1 and Th17 responses, to further clear apoptotic cells, and to repair intestinal epithelium.

There exists increasing evidence that defects in both macrophage efferocytosis and macrophage reprogramming may be involved in the pathogenesis of IBD. Following efferocytosis of apoptotic cells, LP macrophages overexpressed genes overlapping with 41 susceptibility loci for IBD[17]—suggesting a role for efferocytosis in IBD. In addition, an analysis of genome-wide association studies concluded that IBD susceptibility loci were enriched for promoters involved in macrophage differentiation.[18] Furthermore, human intestinal immature inflammatory macrophages, rather than tolerogenic mature macrophages, are expanded in IBD.[19] As a result, efferocytosis and reprogramming offer possible targets for the treatment of IBD. Several new therapies that seek to promote the differentiation of immature macrophages into resolving macrophages are currently under consideration.[14]

We investigate here the role of macrophage COX2 in primary efferocytosis and in efferocytosis-dependent macrophage reprogramming, including intestinal epithelial repair capacity. We report that COX2 potentiates the primary efferocytosis capacity of mouse macrophages, in part by promoting their binding capacity for apoptotic cells. We also find that COX2 modulates several aspects of resolution reprogramming: COX2 mediates the production of efferocytosis-dependent lipid inflammatory mediators that include the eicosanoids prostaglandin (PG) I2, PGE2, LXA4, and 15d-PGJ2; potentiates macrophage secondary efferocytosis capacity; and mediates the efferocytosis-dependent capacity of macrophages to augment and amplify intestinal epithelial repair. We suggest that these findings identify a potential target for enhancing the resolving phenotype and function of macrophages in a manner that may prove protective against IBD.

Results

Cox2 MKO modulates both the degree and character of ileo-ceco-colic inflammation in mice fed a CCHF diet

Both *Cox2* MKO and control *Cox2* floxed (FLOX) mice were fed a CCHF diet for 10 weeks. The degree of intestinal inflammation in histological cross-sections of the ileo-ceco-colic regions from these mice was determined (Figure 1*A*). Consistent with our prior report,[5] MKO mice possessed approximately 30-fold more inflammation by % area than FLOX mice. The neutrophil-to-macrophage ratio for MKO and FLOX in regions of comparable macrophage burden was also determined (Figure 1*B* and *C*). MKO mice exhibited a significantly higher neutrophil-to-macrophage ratio, compared with FLOX mice, within these macrophage-high inflammatory regions. We conclude that, in mice fed the CCHF diet, *Cox2* MKO alters not only the degree of intestinal inflammation, but also its character.

COX2 modulates the efferocytosis capacity of mouse macrophages

The comparative failure of *Cox2* MKO macrophages to clear neutrophils within inflammatory regions (Figure 1) is consistent with dysregulated macrophage efferocytosis capacity.[13] In addition, we previously observed that *Cox2* MKO and chronic COX2 inhibition increased the inflammatory response of LPS-activated murine macrophages.[5]

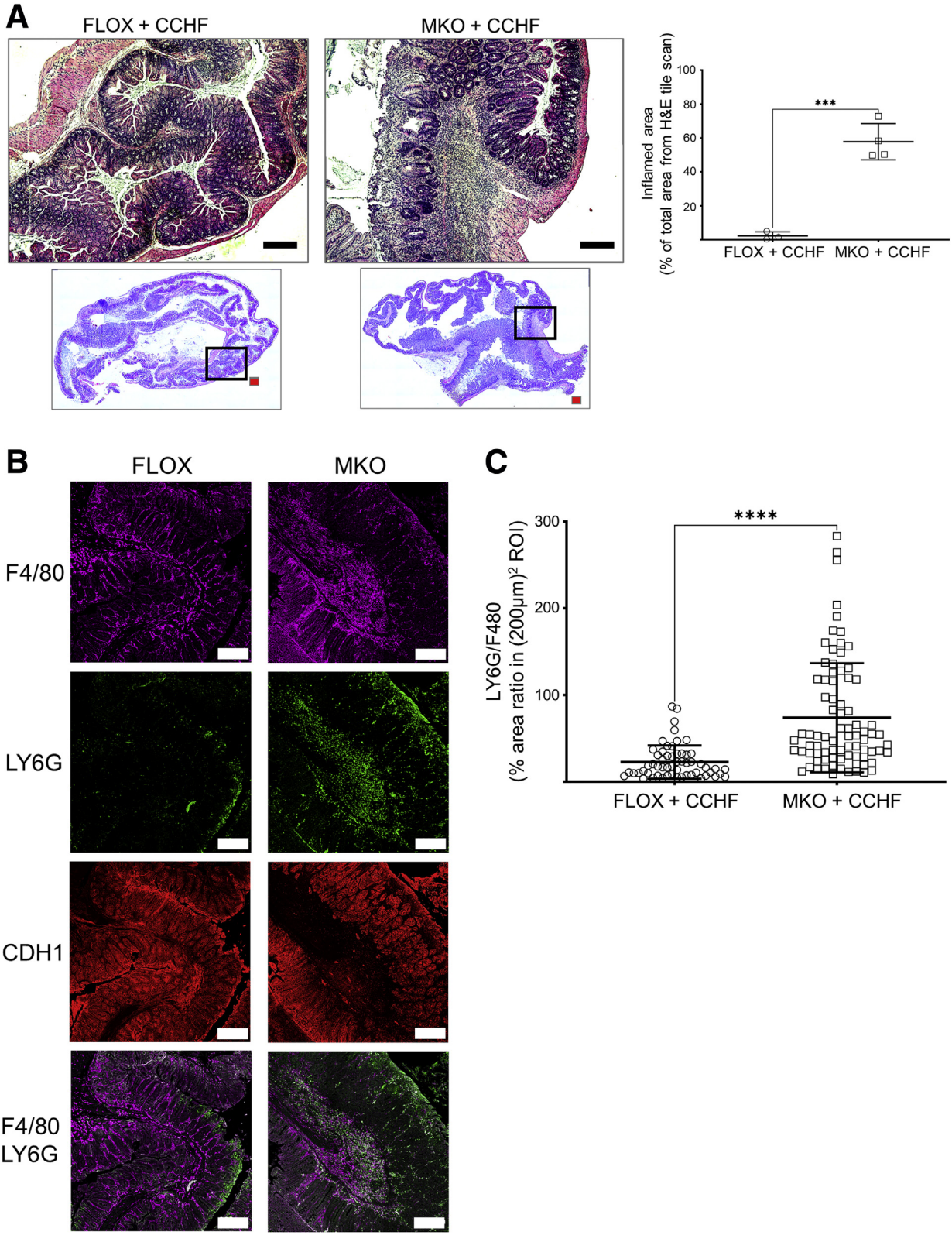

Inflammatory macrophages (so-called classically activated or M1 macrophages) possess less efferocytosis capacity than either unpolarized macrophages (M0) or those that promote inflammation resolution and wound repair (so-called alternatively activated or M2 macrophages).[20] Consequently, we hypothesized that both *Cox2* MKO and chronic COX2 inhibition would impair the efferocytosis capacity of murine macrophages.

The efferocytosis capacity of macrophages can be quantitatively assayed with labeled apoptotic immune cells or labeled phosphatidylserine (PS)-coated synthetic apoptotic bodies.[20] Efferocytosis capacity was first assessed by determining the number of labeled apoptotic murine neutrophils bound or internalized by murine macrophages.

MPRO cells are a granulocyte-macrophage colony-stimulating factor (CSF) dependent, immortalized neutrophil progenitor line that exhibits a number of neutrophil characteristics that include cell surface expression of mouse neutrophil-specific antigen 7/4.[21] Both 1 μM staurosporine and heat shock at 43°C[20] were tested for effectiveness at inducing apoptosis in MPRO cells. The degree of MPRO cell apoptosis was determined by annexin V-FITC staining. Staurosporine was more effective than heat shock (data available upon request). Apoptotic MPRO (apMPRO) cells were labeled with Cell Proliferation Dye eFluor 450—a violet, fluorescent live cell dye that binds to any cellular protein containing primary amines—for subsequent efferocytosis assays.

The efferocytosis capacity of mouse thioglycolate-elicited peritoneal macrophages (PMs) was investigated first. Thioglycolate-elicited PMs are more inflammatory than resident PMs in response to LPS activation[22] and thus better model the inflammatory macrophages that associate with intestinal inflammation[19] that we observed in our prior study.[5] Moreover, only continuous COX2 inhibition with SC236 across 7 days but not across 2 days (chronic COX2 inhibition) significantly increased the LPS-dependent inflammatory response of PMs compared with COX2 uninhibited control cells (Figure 2*A*). PMs from day 7 with and without chronic COX2 inhibition were nonetheless as viable as 2-day controls (Figure 2*B*). In addition, both 7-day and 2-day COX2-uninhibited PMs responded comparably to LPS (Figure 2*A* and *C*), suggesting that the additional days in culture did not as such result in loss of function. Consequently, PMs from day 7, rather than from day 2, of culture were employed throughout.

The number of bound or internalized apMPRO cells per PM was determined for PMs from *Cox2* MKO and FLOX mice cultured for 7 days and treated with labeled apMPRO cells for 30, 60, and 90 minutes. Both 60- and 90-minute incubations significantly increased the apMPRO-to-PM ratio compared with 30 minutes for FLOX PMs; deletion of COX2 in MKO cells significantly decreased the apMPRO-to-PM ratio at both later time points (Figure 3*A*). Chronic pharmacologic COX2 inhibition also reduced the efferocytosis capacity of 7-day PMs (Figure 3*B* and *C*).

We also asked whether loss of COX2 would impair the efferocytosis capacity of macrophages that exhibited a more inflammation resolving phenotype than PMs. Bone marrow–derived macrophages (BMDMs) can be pushed into a resolving phenotype through several means, following their differentiation from bone marrow derived monocytes by macrophage CSF. First, IL-10 polarizes BMDMs to a type of alternatively activated phenotype associated with inflammation resolution (viz. M2c); these M2c macrophages exhibit enhanced efferocytosis capacity when compared with either classically activated M1 macrophages or IL-4–activated M2a macrophages (more closely associated with wound repair).[23] Second, low-dose LPS (10 ng/mL over 48 hours) can also induce a partial resolution-like phenotype in mouse macrophages. LPS stimulates IL-10 secretion within 24 hours after addition, and IL-10 can signal in autocrine fashion.[24] Third, even BMDMs that are differentiated in macrophage CSF but are otherwise not polarized (so-called M0 macrophages), express M2 markers,[25] and exhibit M2c-like efferocytosis capacity.[20]

The effect of *Cox2* MKO on the efferocytosis capacity of unpolarized (no treatment [NT]), IL-10–polarized (IL-10), and 10-ng/mL low-dose LPS polarized (10 ng LPS) BMDMs was determined (Figure 4). Absence of COX2 significantly suppressed the binding and internalization of apMPRO cells for all 3 groups (Figure 4*A* and *C*). Chronic COX2 inhibition across both BMDM differentiation and polarization significantly and comparably suppressed efferocytosis of apMPRO cells (Figure 4*B*).

Figure 1. (***See previous page***). **Absence of myeloid COX2 modulates the degree and character of ileo-ceco-colic inflammation in mice fed a CCHF diet.** Four-to-6 month old *Cox2* MKO and *Cox2* FLOX control mice were fed a CCHF diet for 10 weeks (n = 3–4/group). The ileo-ceco-colic regions were fixed in formaldehyde, and paraffin-embedded cross sections were prepared for histological analysis. (*A*) Left panels show cross-sections from each ileo-ceco-colic region stained with hematoxylin and eosin, and tiled micrographs were generated. Representative images from FLOX and MKO mice are shown. Red scale bars = 1 mm. Black scale bars = 250 μm. Black boxes = areas of magnification. The right panel shows the % total tissue area of intestinal inflammation within each cross-section determined in FIJI. (*B*) Cross-sections were probed with antibodies against the epithelial marker CDH1, the neutrophil marker LY6G, and the macrophage marker F4/80; tiled confocal micrographs were generated. Representative micrographs taken of comparable F4/80-positive regions in both MKO and FLOX cross-sections are shown. White scale bar = 200 μm. Imaging was performed on a Zeiss LSM 900 confocal microscope as described in the Materials and Methods. (*C*) Tiled micrographs of comparable F4/80-positive regions within each MKO and FLOX cross-section were analyzed in FIJI. The % area ratio of LY6G to F4/80-positive fluorescence was determined in 15–20 (200 μm)^2 regions of interest (ROIs) within each micrograph. ***$P < .001$; ****$P < .0001$. Unpaired Student's *t* tests.

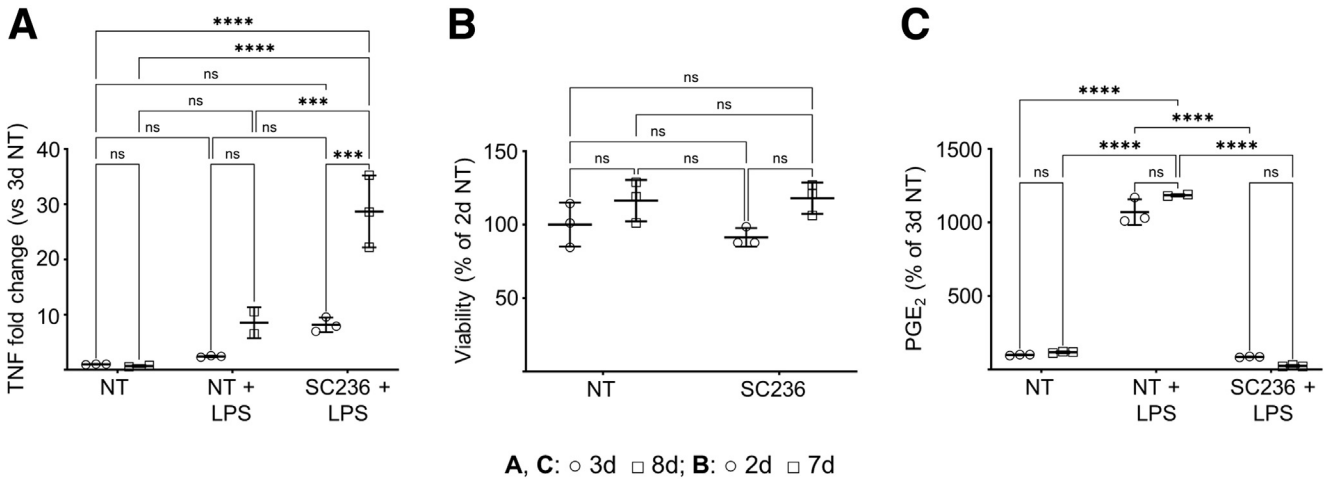

Figure 2. Chronic COX2 inhibition across 7 days, but not 2 days, increases the LPS-dependent inflammatory response of murine PMs; while seven days of culture does not otherwise affect PM viability or PM function. (*A*) PMs from BL6 mice were treated with vehicle (NT) or the COX2 inhibitor SC236 for 2 or 7 days. LPS (100 ng/mL) or vehicle was then added. Treatment was otherwise maintained, and 24 hours later, TNFα (TNF) gene expression was determined by qPCR on day 3 and day 8. Three biological replicates per condition. (*B*) Cell viability of 2-day and 7-day PMs with and without chronic COX2 inhibition was determined by DAPI exclusion via fluorescence-activated cell sorting. 3 biological replicates per condition. (*C*) LPS-dependent PGE2 levels in the media of the experiment represented in panel *A* were determined by LC-MS/MS. ***$P <$ .001; ****$P <$ .0001. Two-way analysis of variance with Tukey's multiple comparisons test and adjusted *P* values. d, day; ns, not significant.

COX2 modulates efferocytosis in part by affecting the binding capacity of macrophages for apoptotic neutrophils

Macrophage efferocytosis in vivo consists of 3 stages: apoptotic cell finding, apoptotic cell binding, and apoptotic cell internalization and degradation.[26] The in vitro efferocytosis assay described in Figures 3 and 4 cannot interrogate apoptotic cell finding: apoptotic neutrophils are added directly to cultured macrophages. Thus, the inhibitory effects associated with Figures 3 and 4 must reflect differences of apoptotic cell binding or apoptotic cell internalization. We next investigated whether macrophage COX2 loss reduces the binding capacity for apoptotic neutrophils (Figure 5).

Apoptotic cell internalization begins when engagement of cell surface receptors on efferocytes activates the RHO family of GTPases, including RAC1, to mediate apoptotic cell internalization.[26] Upon activation, RAC1 localizes to the apoptotic cell engagement site on the plasma membrane where, through several steps, actin is polymerized to form the phagocytic cup, leading to apoptotic cell internalization.[26] Inhibition of actin polymerization, by pretreating macrophages with the mycotoxin cytochalasin D, prevents apoptotic cell internalization.[27] With internalization blocked, any differences in the association of macrophage populations with apMPRO cells would be due to differences in macrophage apoptotic cell binding capacity.

BMDMs generated from *Cox2* MKO and control FLOX mice were polarized as described previously. The BMDMs were pretreated with 5 μM cytochalasin D for 30 minutes then assayed at 60 minutes for association between apMPRO cells and BMDMs. As expected, cytochalasin D blocked apMPRO cell internalization. However, COX2 absence in macrophages significantly suppressed the binding of apMPRO cells for all 3 groups of BMDMs (NT, IL-10, and 10 ng LPS) (Figure 5*A* and *D*). Chronic pharmacologic COX2 inhibition also reduced the binding capacity of BMDMs (Figure 5*B*) and PMs (Figure 5*C*) for apMPRO cells.

Loss of COX2 activity suppresses efferocytic index in a manner comparable to M1 polarization

When cells undergo apoptosis, they externalize PS to their outer cell membrane. Efferocytes can bind to apoptotic cells by binding to this PS directly, or through bridge molecules that bind membrane-associated PS.[26] It is possible to generate synthetic apoptotic targets that consist of silica beads coated with PS and phosphatidylcholine (PC). Macrophages will bind and internalize these PS/PC liposomes as if they were apoptotic cells.[20] By adding to the PS/PC liposomes both phosphatidylethanolamine (PE) conjugated to rhodamine and PE conjugated to biotin, it is possible to quantitatively distinguish between liposomes that are bound to macrophages and liposomes that have been internalized by the macrophages.[20] The liposomes are always rhodamine positive; however, they can acquire a second color if bound to a labeled streptavidin. Streptavidin, however, cannot enter unpermeabilized cells. Thus, if streptavidin is added prior to fixation and permeabilization, liposomes bound to the cell surface but not yet internalized will contain 2 colors. By contrast, internalized liposomes will only be rhodamine positive. The number of internalized apoptotic bodies per efferocyte, called the efferocytic index, is a measure of efferocytosis capacity. The number of internalized apoptotic bodies as a percent of the total number of bound and internalized apoptotic bodies, called efferocytic

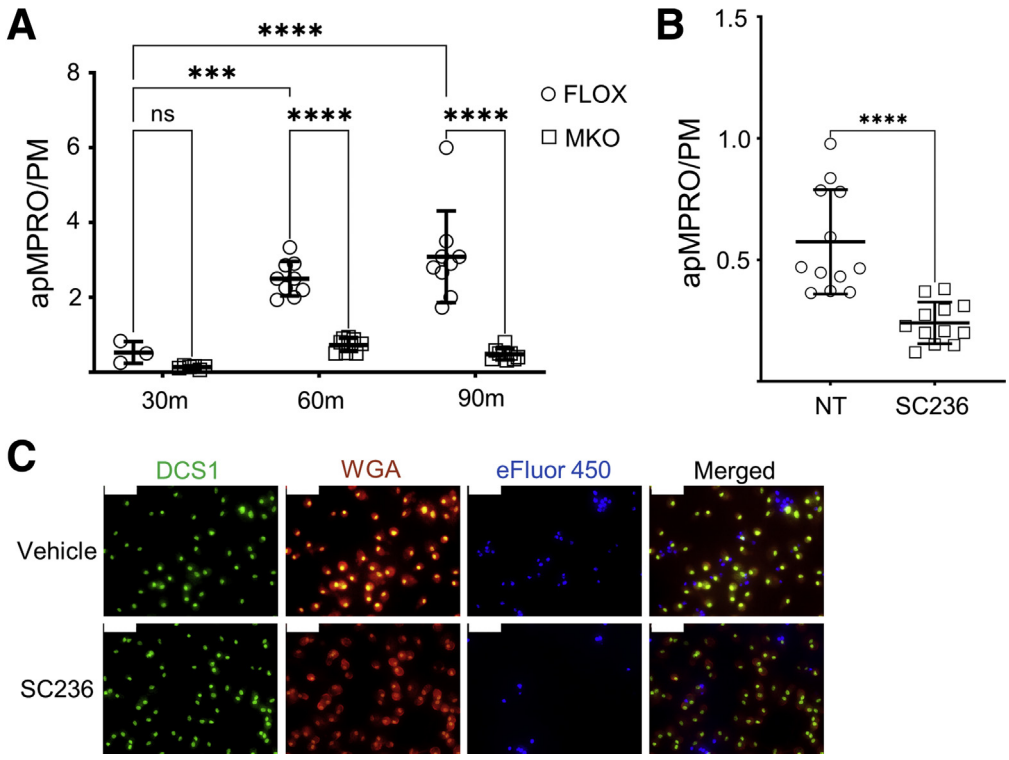

Figure 3. COX2 modulates the efferocytosis of apoptotic neutrophils by murine PMs. (*A*) Thioglycolate-elicited PMs isolated from *Cox2* MKO and control FLOX mice were cultured for 7 days. To assess the efferocytosis capacity of the PMs, murine MPRO neutrophils were first treated with staurosporine to induce apoptosis, then labeled with Cell Proliferation Dye eFluor 450. Labeled apMPRO cells were added to the macrophages, and the numbers of cell-associated apMPRO per PM were determined at 30, 60, and 90 minutes. (*B*) PMs isolated from BL6 mice were either treated with vehicle (NT) or the COX2 inhibitor SC236 for 7 days, then treated with labeled apMPRO cells. The numbers of cell-associated neutrophils per PM were determined after 60 minutes. (*C*): For all analyses in panels *A* and *B*, up to 12 fields of approximately 100 macrophages each were analyzed from 3 separate biological replicates per condition. Data are shown for the experiment in panel *B*. PM cell numbers were determined by staining with nuclear green DCS1 and wheat germ agglutinin (WGA) Texas Red-X conjugate. apMPRO cell numbers were determined by prestaining with Cell Proliferation Dye eFluor 450. ×40 magnification; representative images are shown. Scale bar = 50 μm. *$P < .05$; **$P < .01$; ***$P < .001$; ****$P < .0001$. (*A*) One-way analysis of variance with Tukey's multiple comparisons test and adjusted *P* values. (*B*) Unpaired Student's *t* tests. m, minutes.

efficiency, is a measure of the efficiency of internalization following binding.[20] This scheme is illustrated in Figure 6*A*. While the efferocytic index is a function of both binding and internalization capacities, efferocytic efficiency more directly assesses internalization capacity alone.

The effect of COX2 on the efferocytic index and the efferocytic efficiency of variously polarized BMDMs was determined. BL6 BMDMs were chronically COX2 inhibited with SC236 or left uninhibited (wild-type [WT]). BMDMs were either unpolarized (NT), polarized with IL-10 (IL-10), or polarized with 10-ng/mL low-dose LPS (10 ng LPS). Because M1 polarization suppresses the efferocytic index and efferocytic efficiency compared with M0 and M2 polarizations,[20] additional BMDMs were polarized with 100-ng/mL high-dose LPS (100 ng LPS) to serve as M1-polarized negative control cells. BMDMs were challenged with PC/PS/PE-rhodamine/PE-biotin liposomes; streptavidin AF-635 was added; the cells were stained and fixed; and the fixed cells were imaged with a confocal microscope.

The efferocytic index of WT BMDMs was significantly reduced by 100 ng LPS compared with NT. Chronic COX2 inhibition with SC236 also significantly reduced the efferocytic index of BMDMs for NT, IL-10, and 10 ng LPS groups compared with WT. The effects of 100 ng LPS and SC236 on efferocytic index were comparable. In contrast, SC236 did not affect the efferocytic index of 100 ng LPS–treated BMDMs ($P = .4$) (Figure 6*B* and *D*). The efferocytic efficiency of both WT and SC236-treated BMDMs was significantly reduced by 100 ng LPS compared with 10 ng LPS BMDMs, but COX2 inhibition did not significantly reduce the efferocytic efficiency in NT, IL-10, and 10 ng LPS groups (Figure 6*C*). These results suggest that loss of COX2 inhibits efferocytosis by affecting apoptotic cell binding without necessarily affecting apoptotic cell internalization as such.

Loss of COX2 biases macrophage differentiation phenotype and inhibits induction of genes expressed in efferocytosis-competent macrophages

Chronic COX2 inhibition and *Cox2* MKO both reduced macrophage efferocytosis capacity. In contrast, COX2

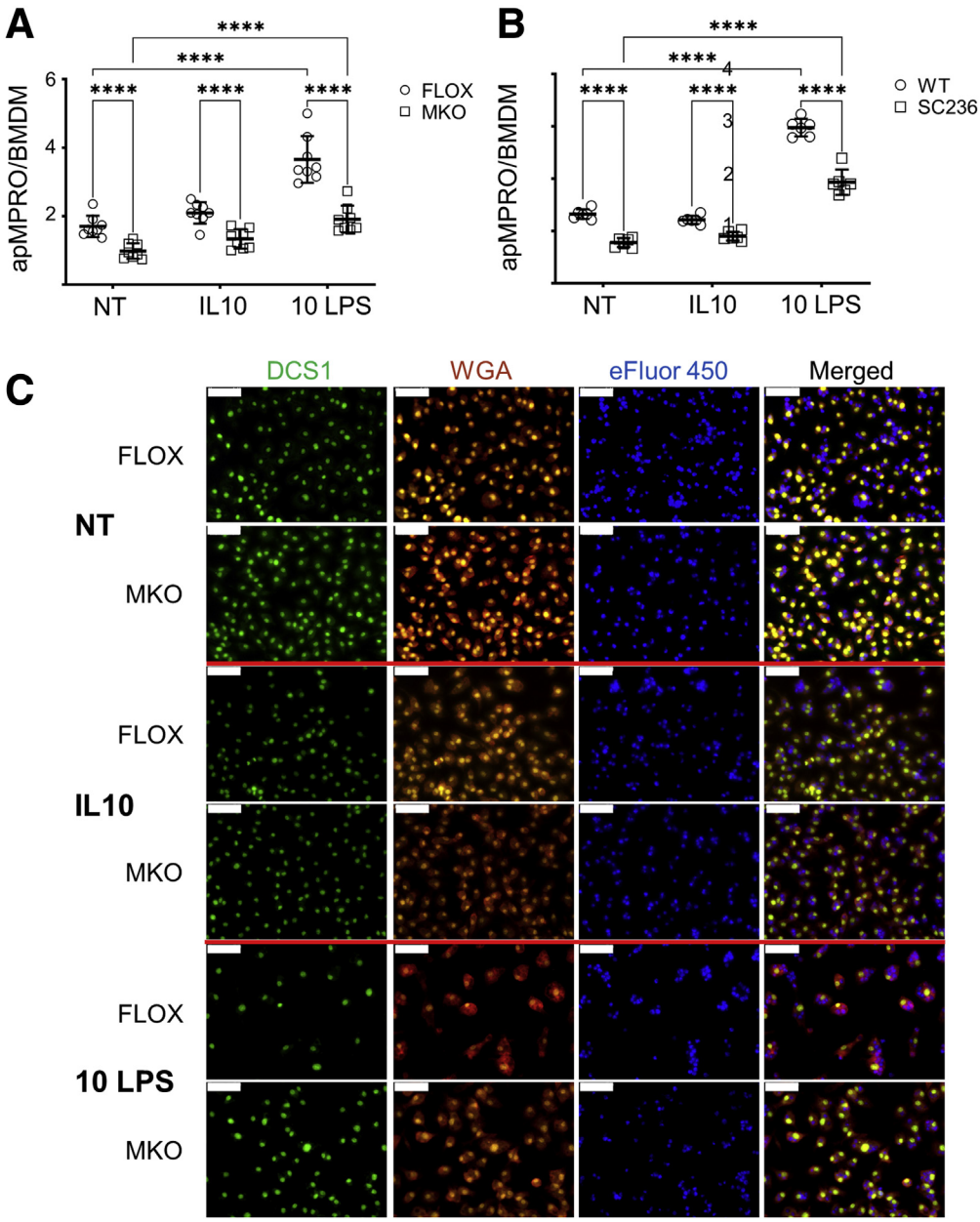

Figure 4. COX2 modulates the efferocytosis of apoptotic neutrophils by murine BMDMs. (*A*) BMDMs were derived from *Cox2* FLOX and *Cox2* MKO mice. Cells were either left unpolarized (NT) or treated for 48 hours with 20 ng/mL IL-10 (IL-10) or 10 ng/mL LPS (10 LPS). Labeled apMPRO cells were added for 60 minutes, and the number of neutrophils per macrophage was determined. (*B*) Chronically COX2 inhibited (SC236) or uninhibited (WT) BMDMs derived from BL6 mice were treated and assessed comparably. (*C*) Representative data for NT or IL-10– and LPS-treated cells from the experiment presented in panel *A*. BMDMs were stained with nuclear green DCS1 and WGA Texas Red-X conjugate, while MPRO cells were prestained with Cell Proliferation Dye eFluor 450. ×40 magnification; representative images. Scale bar = 50 um. For panels *A* and *B*, six to 8 fields of approximately 100 macrophages each were analyzed from 3 separate biological replicates per condition. $^{*}P < .05$; $^{**}P < .01$; $^{***}P < .001$; $^{****}P < .0001$. Two-way analysis of variance with Tukey's multiple comparisons test and adjusted *P* values.

inhibition from 60 minutes prior to the addition of apMPRO cells (acute COX2 inhibition) did not alter binding or internalization of apMPRO cells (Figure 7*A*). Chronic COX2 inhibition biases macrophage phenotype toward an inflammatory M1 state.[7,8] Inflammatory M1 macrophages exhibit less efferocytosis capacity than either M0 or M2c macrophages.[20] We thus considered the possibility that chronic or constitutive COX2 loss impairs macrophage efferocytosis by biasing macrophage phenotype during differentiation or polarization.

Prostanoid levels in the media on day 4 of differentiating BMDM cultures were determined by liquid chromatography tandem mass spectrometry (LC-MS/MS) (Figure 7*B*). Elevated levels of PGE2 and its degradation product 15keto-PGE2, together with 6keto-PGF1α—the degradation product of prostacyclin—were present. Moreover, chronic COX2 inhibition during differentiation significantly reduced the levels of all 3 prostanoids.

Gene expression of common polarization markers was analyzed by quantitative polymerase chain reaction (qPCR) under treatment conditions that induce alternatively activated phenotypes: (1) NT, with its M2 bias in BMDMs,[25] as well as (2) IL-4 (M2a inducing) and (3) IL-10 (M2c-inducing) treatments. Both chronic COX2 inhibition and *Cox2* MKO significantly reduced expression of the M2 marker *Ym1*[28] when compared with their corresponding control cells (Figure 7*C*). The M1 marker inducible *Nos2*, normally expressed at very low levels under IL-4 and IL-10

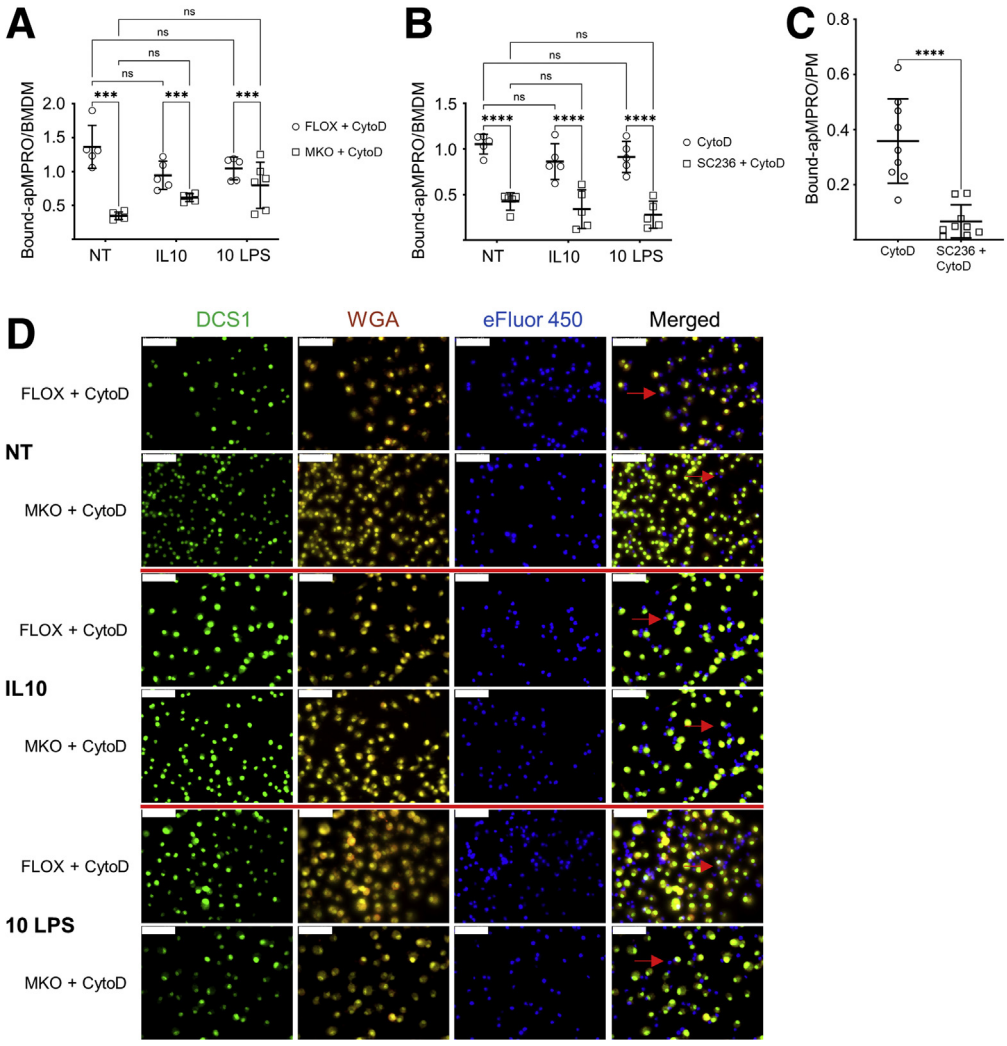

Figure 5. COX2 modulates efferocytosis by BMDMs and PMs in part by affecting the binding capacity for apoptotic neutrophils. For all panels, cytochalasin D (CytoD) was added 30 minutes prior to the addition of apMPRO neutrophils, to prevent the internalization of cell surface bound apoptotic cells. (*A*) FLOX and *Cox2* MKO BMDMs were either left unpolarized (NT) or polarized for 48 hours with IL-10 or low-dose LPS (10 LPS). Binding of apMPRO cells to the surface of CytoD-treated FLOX and *Cox2* MKO macrophages was determined as bound apMPRO per BMDM. (*B*) BMDMs isolated from BL6 mice were treated and assessed as described for panel *A*, with the exception that COX2 was chronically inhibited with SC236. (*C*) Thioglycolate-elicited PMs from BL6 mice were treated with vehicle or SC236 for 7 days, and the PM binding capacity for apMPRO was determined as in panel *A*. (*D*) Representative data from the experiment presented in panel *A*. BMDMs were stained with nuclear green DCS1 as well as with the cell membrane dye WGA Texas Red-X conjugate; MPRO cells were stained with Cell Proliferation Dye eFluor 450. ×40 magnification. Red arrows point to apMPRO cells bound to the macrophage cell membrane, but not internalized. Scale bar = 50 um. For panels *A*–*C*, 5–9 fields were analyzed from 3 biological replicates per condition. **P* < .05; ***P* < .01; ****P* < .001; *****P* < .0001. (*A*, *B*) Two-way analysis of variance with Tukey's multiple comparisons test and adjusted *P* values. (*C*) Student's unpaired *t* test.

treatment,[28] was also significantly increased for all 3 BMDM groups (NT, IL-4, IL-10) by both chronic COX2 inhibition and *Cox2* MKO (Figure 7*D*).

Absence of COX2 reduced both the macrophage binding capacity for apoptotic neutrophils (Figure 5) and the macrophage efferocytic index (Figure 6). These observations suggested that COX2 loss would affect gene expression levels of various components of the cellular machinery involved in efferocytosis. It was next determined whether COX2 inhibition would reduce expression of efferocytosis-specific genes in a manner comparable to high-dose LPS. Chronically COX2-inhibited (SC236) BMDMs and untreated BMDMs (WT) were treated with either IL-10 or 100 ng LPS. Gene expression levels were determined for the direct PS receptors STAB1 and TIM3; the bridge molecules GAS6, MFG-E8, and PROS1; the indirect PS receptors MERTK and AXL; the internalization elements ELMO1 and DOCK1; and RAC1, the GTPase activated by apoptotic cell binding (Figure 8).[26] The 100 ng LPS induced significantly lower expression of several genes involved in apoptotic cell binding compared with IL-10. These genes included the direct PS receptors *Stab1* and *Tim3* (Figure 8*A* and *B*); the

bridge molecules *Gas6* (Figure 8*C*), *Mfge8* (Figure 8*D*), and *Pros1* (Figure 8E); and the indirect PS receptor *Axl* (Figure 8*G*). COX2 inhibition did not alter expression of these genes in response to 100 ng LPS. However, in response to IL-10, COX2 inhibition significantly suppressed expression of *Stab1* (Figure 8A), *Gas6* (Figure 8*C*), and

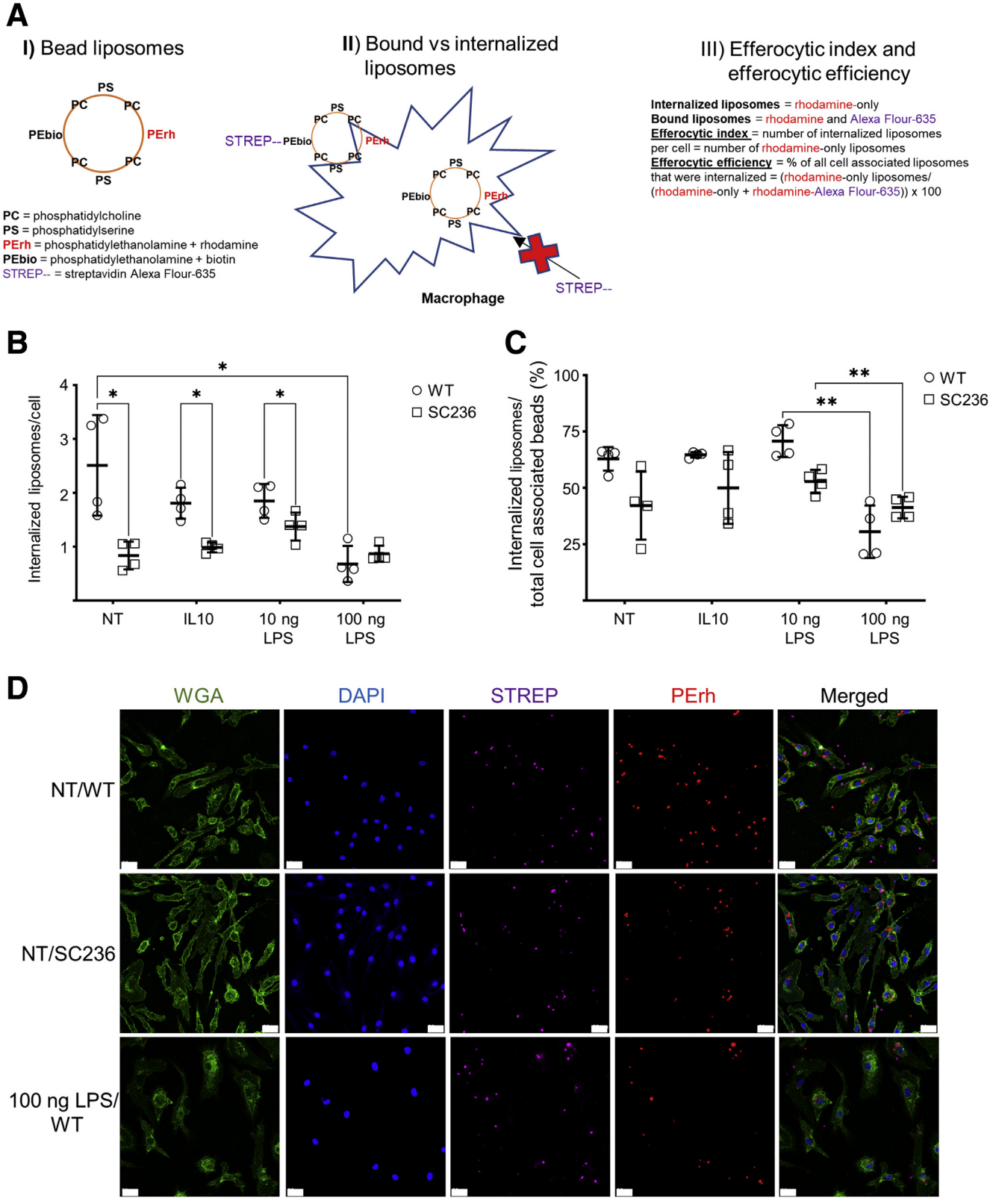

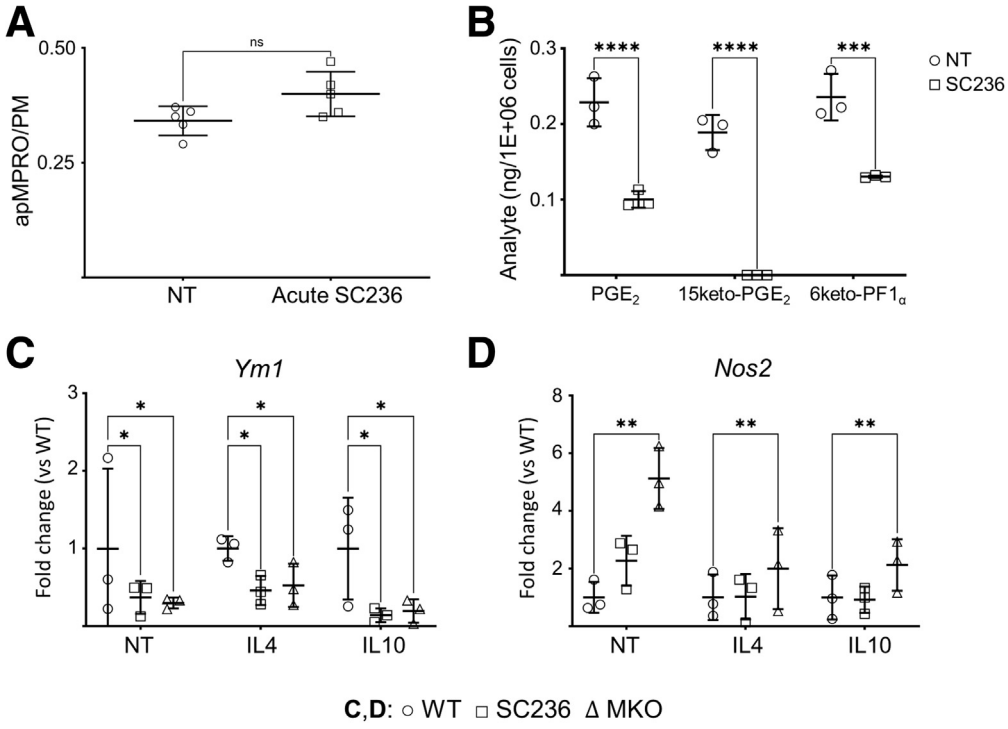

Figure 7. Acute COX2 inhibition does not affect efferocytosis, but chronic or constitutive loss of COX2 activity suppresses prostanoids otherwise present across the differentiation of monocytes into BMDMs while biasing the polarization state of BMDMs toward an inflammatory phenotype. (*A*) BL6 PMs were culture for 7 days and then pretreated with vehicle (NT) or SC236 for 60 minutes prior to addition of labeled apMPRO cells. Numbers of apMPRO cells per PM were determined by assessing multiple micrographic fields of at least 200 PMs for 3 biological replicates. (*B*) Bone marrow–derived monocytes were isolated from BL6 mice and treated with vehicle (NT) or the COX2 inhibitor SC236 from time 0. Media collected on day 4 were analyzed by LC-MS/MS for eicosanoids including PGE2, the PGE2 degradation product 15keto PGE2, and the PGI2 degradation product 6ketoPGF1α. Data from 3 biological replicates. (*C*, *D*) Bone marrow–derived monocytes from BL6 and *Cox2* MKO mice were treated with vehicle or SC236 from time 0 (WT = BL6 BMDM + vehicle; SC236 = BL6 BMDM + SC236; MKO = *Cox2* MKO BMDM + vehicle). On day 8, BMDMs were further treated with vehicle, IL-4 (20 ng/mL), or IL-10 (20 ng/mL). On day 10, gene expression levels of the activation markers *Ym1* (M2/M2a marker) and *Nos2* (M1 marker) were determined by qPCR. Data are expressed as fold differences from the corresponding intragroup COX2 WT and uninhibited control (WT). *$P < .05$; **$P < .01$; ***$P < .001$; ****$P < .0001$. (*A*) Unpaired Student's *t* test. (*B–D*) 2-way analysis of variance with Tukey's multiple comparisons test and adjusted *P* values. ns, not significant.

Mfge8 (Figure 8*D*). These reductions in expression of genes related to the direct and indirect binding of PS may explain why loss of COX2 reduces the binding capacity of macrophages for apoptotic neutrophils. Reduction in binding capacity, but not in expression of cellular machinery associated with internalization, may explain why COX2 loss reduced the efferocytic index without significantly altering efferocytic efficiency—without, in order words, seemingly altering the capacity of macrophages to internalize apoptotic cells once they are surface bound. See Figure 8*K* for a summary of the genes analyzed.

Efferocytosis triggers the production of COX- and lipoxygenase-dependent lipid signaling mediators in macrophages

COX2 and PGE2 are induced in murine macrophages by exposure to apoptotic cells, and apoptotic cell–dependent

Figure 6. (***See previous page***). **BMDM COX2 inhibition suppresses efferocytic index in a manner comparable to M1 polarization.** BMDMs derived from BL6 mice were chronically inhibited with SC236 from isolation or left uninhibited (WT). BMDMs were left unpolarized (NT) or polarized with IL-10, low-dose LPS (10 ng LPS), or high-dose LPS as an M1 control (100 ng LPS). After 48 hours, synthetic apoptotic targets (silica beads coated with PC, PS, PE conjugated to rhodamine, and PE conjugated to biotin) were added to the macrophages. After 45 minutes, streptavidin Alexa Fluor-635 together with DAPI to stain nuclei and WGA Alexa Fluor-488 conjugate to stain cell membranes were added; and the cells were fixed with paraformaldehyde. (*A*) Schematic for the determination of efferocytic index (the number of internalized liposomes per cell) and efferocytic efficiency (% of all cell associated liposomes that were internalized) using the 2-color liposomal bead assay. (*B*, *C*) Both efferocytic index and efferocytic efficiency were determined from confocal micrographs by independently averaging the scores of 4–6 micrographs from each of 4 biological replicates. (*D*) Representative fluorescent images for data in panels *B* and *C*. Imaging was performed on a Zeiss LSM 900 confocal microscope as described in the Materials and Methods. Image analysis was performed using ImageJ. Scale bar = 20 um. *$P < .05$; **$P < .01$; ***$P < .001$; ****$P < .0001$. Two-way analysis of variance with Tukey's multiple comparisons test and adjusted *P* values.

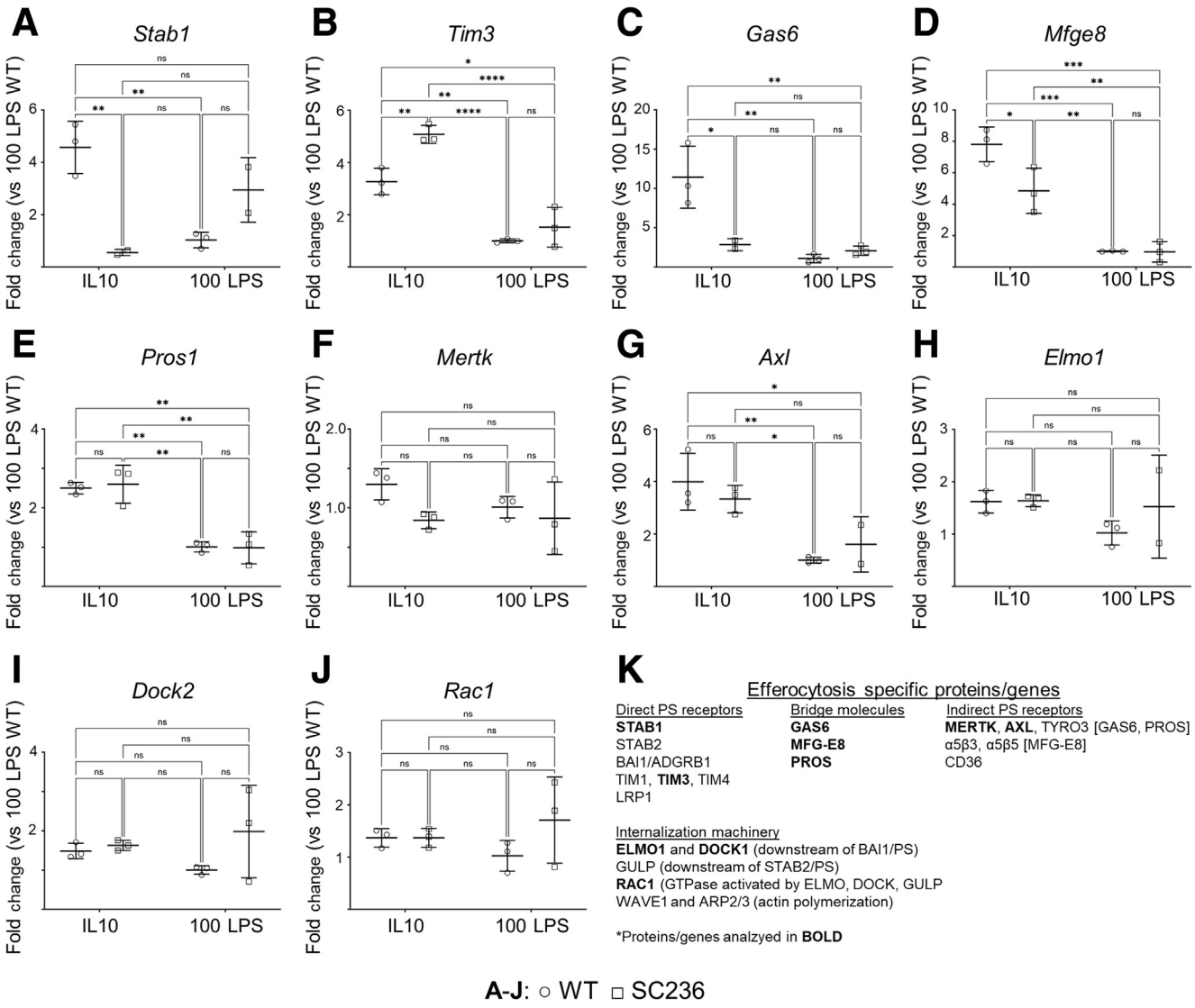

Figure 8. Chronic COX2 inhibition reduces macrophage expression of efferocytosis-specific genes. BL6 BMDMs were treated with vehicle (WT) or the COX2 inhibitor SC236 from isolation. On day 8, BMDMs were polarized with either 20 ng/mL IL-10 (IL-10) or 100 ng/mL LPS (100 LPS). (*A–J*) Expression of efferocytosis-specific genes on day 10 of culture was determined by qPCR. Data are presented as fold change compared with WT COX2 + 100 ng/mL LPS. (*K*) Summary of efferocytosis specific proteins whose associated gene expression was investigated by qPCR. **P* < .05; ***P* < .01; ****P* < .001; *****P* < .0001. Two-way analysis of variance with Tukey's multiple comparisons test and adjusted *P* values. ns, not significant.

PGE2 can modulate, in an autocrine fashion, the production and release from mouse macrophages cellular growth factors, including hepatocyte growth factor.[29] We thus hypothesized that COX2 would modulate several aspects of efferocytosis-dependent macrophage reprogramming, including intestinal epithelial repair.

Eicosanoids released by PMs in response to efferocytosis were determined by scheduled multiple reaction monitoring LC-MS/MS.[5] BL6 PMs were treated with apMPRO cells and apMPRO cells + cytochalasin D. To isolate the effect of COX2 only during apMPRO-dependent macrophage response, PMs were treated with apMPRO cells + acute SC236. Media were sampled over a 32-hour period, during which time the cultures were maintained in lipoprotein-deficient fetal bovine serum (FBS).

Efferocytosis enhanced the production of multiple eicosanoids (Figure 9*A*), significantly increasing at 32 hours the levels of the prostanoids PGE2 and PGD2 (Figure 9*B*), as well as degradation products of PGE2, PGD2, PGI2, and PGF2α (Figures 9*C*). Efferocytosis also significantly increased the levels of 2 anti-inflammatory and inflammation resolving eicosanoids, LXA4 and 15d-PGJ2 (Figure 9*D*). Efferocytosis significantly increased levels of the monohydroxylated arachidonic acid (AA) products 15HETE, 5HETE, and 11HETE as well (Figure 9*E*).

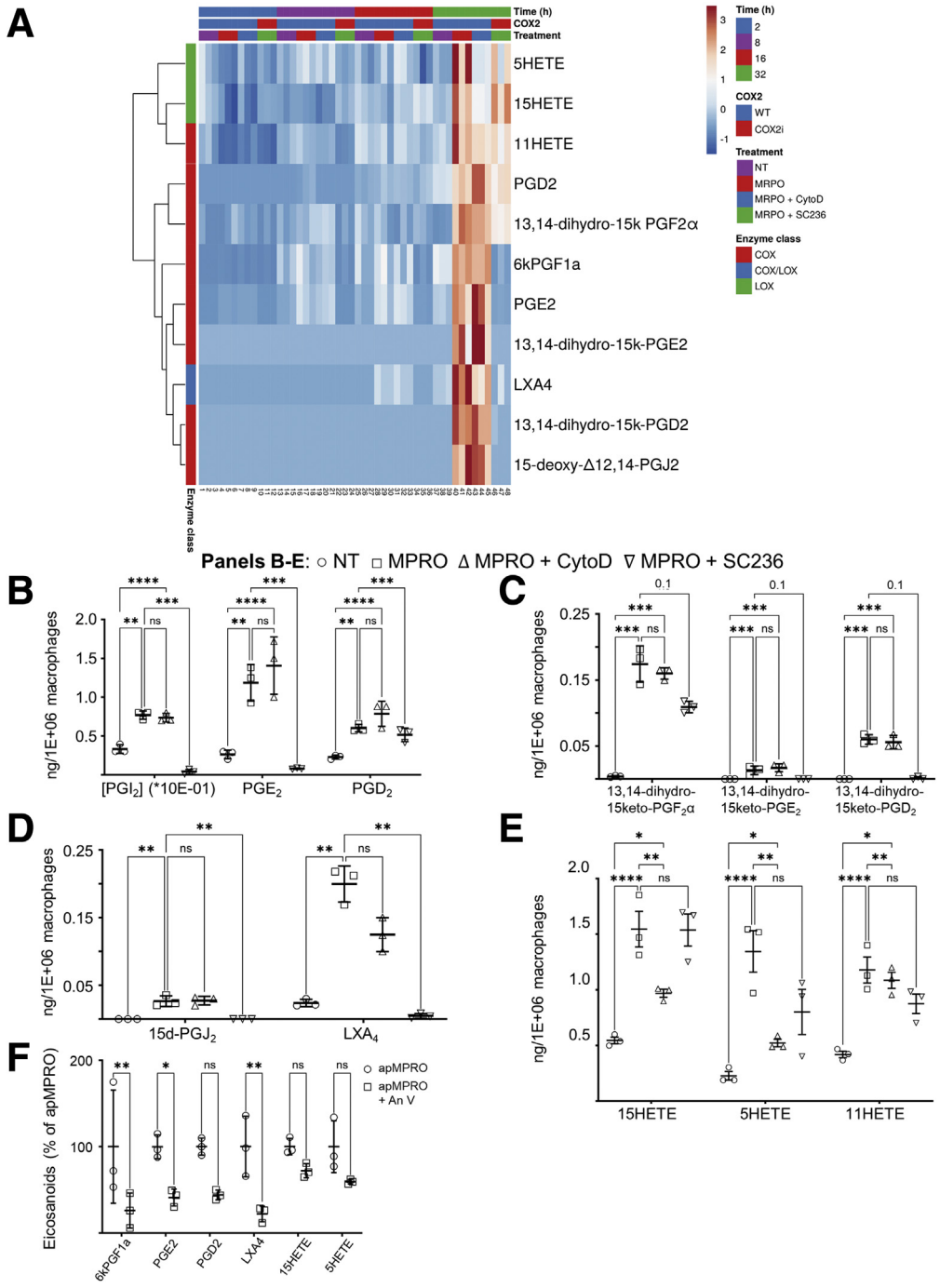

Figure 9. Efferocytosis triggers production of COX- and lipoxygenase-dependent lipid signaling mediators in macrophages. (*A*) Mouse PMs were treated with apoptotic mouse neutrophils (MPRO cells), together with the inhibitors CytoD and SC236; eicosanoid levels in media were determined by LC-MS/MS across 32 hours (3 biological replicates per time point per condition). Rows were clustered using correlation distance and average linkage. (*B–E*) Efferocytosis triggered the production of (*B*) COX-dependent prostanoids including PGI2 (measured as its degradation product 6ketoPGF1α), PGE2, and PGD2; (*C*) additional prostanoid degradation products; (*D*) anti-inflammatory and inflammation resolving eicosanoids 15dPGJ2 and LXA4; and (*E*) 15HETE, 5HETE, and 11HETE. *$P <$ .05; **$P <$ .01; ***$P <$ .001; ****$P <$ .0001. The Benjamini-Hochberg procedure was applied to 1-way analysis of variance for each lipidomic analyte with false discovery rate at level $\alpha = 0.05$, followed by 2-way analysis of variance with Tukey's multiple comparisons test and adjusted *P* values.

The efferocytosis dependence of these products was further validated by determining the effect of recombinant murine annexin V (AnV) on the levels of these species following induction by apMPRO cells. AnV can bind to PS and block the binding of PS to macrophages.[30] AnV pretreatment of apMPRO reduced the binding and uptake of apMPRO cells by approximately 50% (data available upon request). AnV pretreatment also caused a comparable reduction in apMPRO-dependent eicosanoids (Figure 9*F*). These results support the suggestion that apMPRO-dependent eicosanoids are induced by efferocytosis itself.

The prostanoids and their degradation products are COX-dependent metabolites of AA. The selective COX2 inhibitor SC236 significantly reduced PGE2 and PGD2 levels, indicating a role for COX2 (Figure 9*B*). SC236 also reduced the anti-inflammatory eicosanoid 15d-PGJ2, a derivative of PGD2 (Figure 9*D*). The anti-inflammatory and inflammation resolving eicosanoid LXA4 was also reduced by SC236 treatment. LXA4 can be produced from AA in

mice by the combined activity of 5 lipoxygenase (ALOX5) and 12/15 lipoxygenase (ALOX15). LXA4 can also be produced in macrophages by ALOX5 acting on the 15HETE derived from COX2.[9] COX2 thus appears to be involved in the efferocytosis-dependent production of LXA4.

Cytochalasin D had a differential effect on the efferocytosis-dependent eicosanoids. None of the COX products that were increased by efferocytosis were reduced by inhibiting apoptotic cell internalization (Figures 9*B*–*D*). This result suggests that PM COX activity is induced simply by the binding of apoptotic cells to macrophages. In contrast, cytochalasin D significantly reduced the levels of both 15HETE and 5HETE (Figure 9*E*)—suggesting that apoptotic cell internalization plays at least some role in triggering the production of these possible lipoxygenase products.

Both acute and chronic COX2 inhibition suppress primary efferocytosis-dependent increase in efferocytosis capacity without affecting opsonin-dependent phagocytosis

Primary efferocytosis increases macrophage secondary efferocytosis capacity[26]; however, the underlying mechanism of this reprogramming is not well understood. LXA4, 15dPGJ2, and PGE2 were all induced by efferocytosis in a COX2-dependent manner (Figure 9). Both LXA4[31] and PGE2[32] can increase efferocytosis directly. Moreover, both 15dPGJ2[33] and PGE2[34] can induce M2 macrophages, which possess greater efferocytosis capacity than do M1 macrophages.[20] We thus hypothesized that loss of COX2 activity would impair the primary efferocytosis-dependent increase in secondary efferocytosis capacity.

The effects of both acute and chronic COX2 inhibition on the primary (1°) and secondary (2°) efferocytosis capacities of murine macrophages were determined. BL6 PMs were first treated with vehicle (NT) or SC236 (chronic SC236) from isolation. On day 7, the media were changed to serum-free Opti-MEM + 0.2% bovine serum albumin (BSA), to avoid the possibility that eicosanoids and other factors variably present in FBS might confound the results.[35,36] PMs were pretreated with vehicle or unlabeled apMPRO cells; and after 24 hours, labeled apMPRO cells were added to all cultures. The numbers of labeled apMPRO cells per PMs were determined as measures of 1° and 2° efferocytosis capacity. In NT PMs, 1° efferocytosis significantly increased 2° efferocytosis capacity. Chronic COX2 inhibition significantly inhibited 1° efferocytosis while also blocking the 1° efferocytosis-dependent increase in 2° efferocytosis capacity (Figure 10*A* and *B*). Chronic COX2 inhibition of murine BMDMs produced comparable results (data available upon request). In contrast, acute COX2 inhibition of COX2 did not suppress 1° efferocytosis capacity (cf. Figure 7*A*). Nonetheless, as with chronic COX2 inhibition, the 1° efferocytosis-dependent increase in 2° efferocytosis capacity was also blocked (Figure 10*C* and *D*). These results suggest that COX2 and COX2-dependent autocrine factors induced by 1° efferocytosis are necessary for the increase in efferocytosis capacity observed in our measures of 2° efferocytosis.

To partially assess whether loss of COX2 activity selectively impaired efferocytosis or affected phagocytosis more generally, the experiment of Figures 10*A* and *B* was repeated except that apMPRO cells were first pretreated in mouse serum to initially opsonize the apoptotic cells (Figure 10*E* and *F*).[20] Unlike efferocytosis, phagocytosis of opsonized apoptotic cells depends on receptors for immunoglobulin-Fc and complement.[37] In contrast to the results for efferocytosis, (1) 1° phagocytosis did not increase 2° phagocytosis, and (2) chronic COX2 inhibition did not affect either measure of the phagocytic capacity for opsonized apoptotic cells.

Absence of COX2 modulates intestinal epithelial proliferation in mice fed a CCHF diet

The efferocytosis of apoptotic neutrophils reprograms inflammatory macrophages toward both inflammation resolving and tissue repair phenotypes.[26] We thus asked whether absence of COX2 affects intestinal epithelial proliferation in our COX2-dependent murine IBD models.[5] *Cox2* total knockout (KO) mice were fed chow (CHOW) or CCHF diets for 2 weeks, and EdU uptake over 24 hours by the intestinal epithelium in the terminal ilea of these mice was determined (Figure 11*A*). While *Cox2* KO did not modulate intestinal epithelial proliferation under homeostasis, it significantly suppressed epithelial proliferative response in the context of intestinal inflammation and barrier damage (see Meriwether et al[5] for our prior characterization of this model). The ileo-ceco-colic cross-sections of the experiment detailed in Figure 1 were also assessed for the degree of proliferation in inflammation-adjacent epithelium (Figure 11*B* and *C*). The level of the proliferation marker KI67 was determined by confocal microscopy in crypts that had been sectioned longitudinally on axis. Crypts from *Cox2* MKO cross-sections had significantly less KI67 expression than did *Cox2* FLOX crypts. These data suggest that dysregulation of macrophage-dependent intestinal epithelial repair contributes to the pathogenic mechanism by which *Cox2* MKO drives intestinal inflammation in this murine model of IBD.

COX2 potentiates macrophage efferocytosis-elicited small intestinal epithelial repair

Macrophages from *Cox2* MKO mice exhibited dysregulated efferocytosis function (Figures 3–6); and intestinal epithelium within inflamed regions of *Cox2* MKO mice fed a CCHF diet exhibited dysregulated proliferation (Figure 11). Because efferocytosis can stimulate macrophage-dependent tissue repair,[26] we directly investigated whether COX2 modulates the intestinal epithelial repair capacity of efferocytic macrophages by assessing the effect of macrophage conditioned media (CM) on tissue repair of small intestinal epithelial organoids (enteroids).

Enteroids in differentiation medium recapitulate the normal growth and partial structure of small intestinal epithelium and contain all intestinal epithelial cell types, including Lgr5+ stem cells, Paneth cells, secretory cells, and enterocytes.[38] Enteroids appear dense and opaque as they develop in Matrigel, and they take on a budding structure as new crypts grow or bud out from the primary core

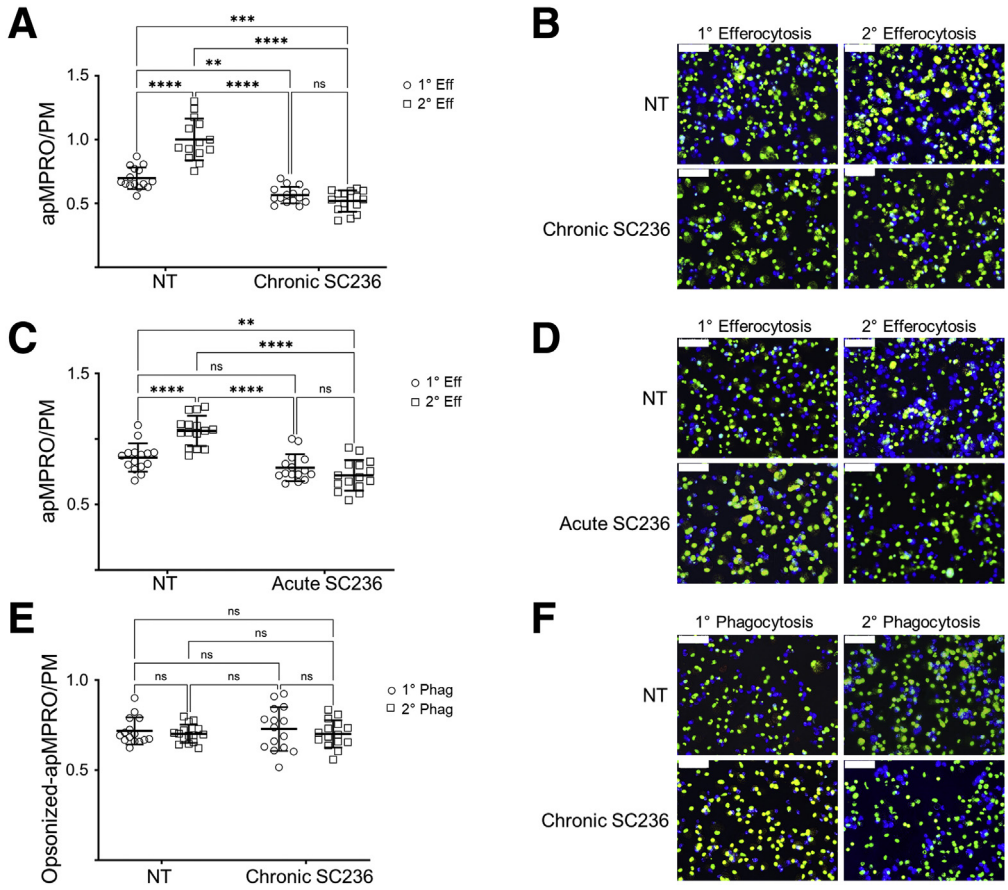

Figure 10. Both chronic and acute COX2 inhibition inhibit primary efferocytosis-dependent increase in efferocytosis capacity without affecting opsonin-dependent phagocytosis. (*A*) Thioglycolate-elicited PMs isolated from BL6 mice were treated from isolation with vehicle (NT) or SC236 (chronic SC236). On day 7, the media were changed to serum free OptiMEM + 0.2% BSA, and PMs were pretreated with vehicle or unlabeled apMPRO cells. After 24 hours, labeled apMPRO cells were added to all cultures, and the numbers of labelled neutrophils per PM at 60 minutes were determined as measures of primary (1° Eff) and secondary efferocytosis (2° Eff) capacity. Five fields of approximately 100 macrophages each were analyzed from each of 3 separate biological replicates per condition. (*B*) Representative data for the assessment presented in panel *A*. PMs were stained with nuclear green DCS1 as well as the cell membrane dye WGA Texas Red-X conjugate, while MPRO cells were stained with Cell Proliferation Dye eFluor 450. ×40 magnification; scale bar = 50 um. (*C*) The prior experiment and analysis were repeated, with the exception that COX2 was acutely inhibited (acute SC236) by addition of SC236 1 hour prior to the addition of the unlabeled or labeled apMPRO cells (for assessment of 2° Eff and 1° Eff, respectively). (*D*) Representative data for the assessment presented in Panel *C*, with staining and microscopy as in panel B. (E) The experiment and analysis presented in panel *A* was repeated, except that apMPRO cells were opsonized in mouse serum for 30 minutes prior to their addition to PMs. Determination in apMPRO to PMs resulted in measures of primary phagocytosis (1° Phag) and secondary phagocytosis (2° Phag). (*F*) Representative data for the assessment presented in Panel *E*, with staining and microscopy as in panels *B* and *D*. $^{**}P < .01$; $^{***}P < .001$; $^{****}P < .0001$. Two-way analysis of variance with Tukey's multiple comparisons test and adjusted *P* values.

(Figure 12*A*).[38] The number of viable structures that develop from isolated crypts or passaged enteroids, and the degree of enteroid budding, are 2 common measures of small intestinal epithelial regenerative or repair capacity.[39,40] Crypts or passaged enteroids can also produce hollow and translucent spherical structures known as spheroids (Figure 12*A*). These spheroids are less differentiated than enteroids, and they can reproduce gene expression patterns and cellular processes associated in vivo with intestinal epithelial restitution.[41,42] Formation of spheroids in differentiation medium has been used as a measure of epithelial plasticity.[43]

We previously used enteroids to interrogate inflammatory crosstalk between TLR-activated macrophages and small intestinal epithelium.[5] Murine enteroids were now employed to assess the role of COX2 in modulating the epithelial repair or regenerative capacity of efferocytic macrophages. PMs from BL6 and *Cox2* MKO mice were cultured either with or without chronic SC236. On day 7, PMs were treated with apMPRO cells or vehicle and maintained in medium containing lipoprotein-deficient FBS. Conditioned media were collected after 24 hours. Enteroids were also grown from crypts isolated from the distal small intestines of BL6 mice.

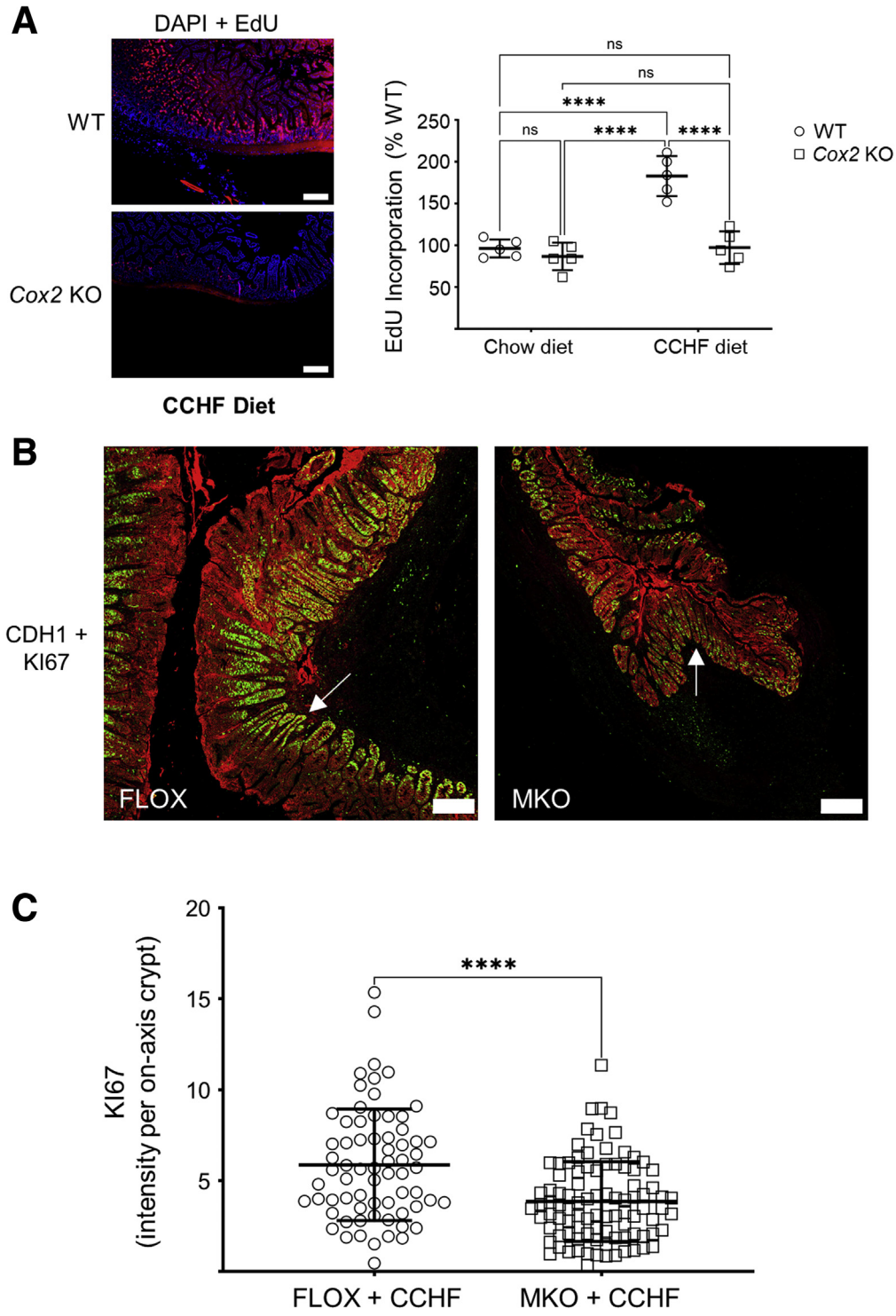

Figure 11. Absence of COX2 modulates intestinal epithelial proliferation in mice fed a CCHF diet. (*A*) *Cox2* KO and BL6 (WT) mice were fed either chow or CCHF diet for 14 days (n = 5/group). EdU was administered 24 hours prior to sacrifice, and longitudinal cross-sections of the terminal ilea from these mice were prepared for histological analysis. Left panel shows representative fluorescent micrographs of these cross-sections. Scale bar = 200 μm. Right panel shows EdU intensity within each cross-section expressed as a percent of WT mean intensity. (*B*, *C*) The ileo-ceco-colic cross-sections from the MKO and FLOX mice in the experiment detailed in Figure 1 were probed with antibodies against the epithelial marker CDH1 (red) and the proliferation marker KI67 (green). Tiled confocal micrographs of comparable inflammation-adjacent epithelial regions were produced. (*B*) Composites of representative KI67 and CDH1 micrographs of FLOX and MKO ileo-ceco-colic cross-sections are shown. Scale bar = 200 μm. White arrows point to crypts sectioned longitudinally on axis. Imaging was performed on a Zeiss LSM 900 confocal microscope as described in the Materials and Methods. (*C*) For every tiled micrograph and each crypt that was longitudinally sectioned on axis, the intensity of KI67-positive fluorescent signal was determined in FIJI. ****$P < .0001$. (*A*) Two-way analysis of variance with Tukey's multiple comparisons test and adjusted *P* values. (*B*) Unpaired Student's *t* test.

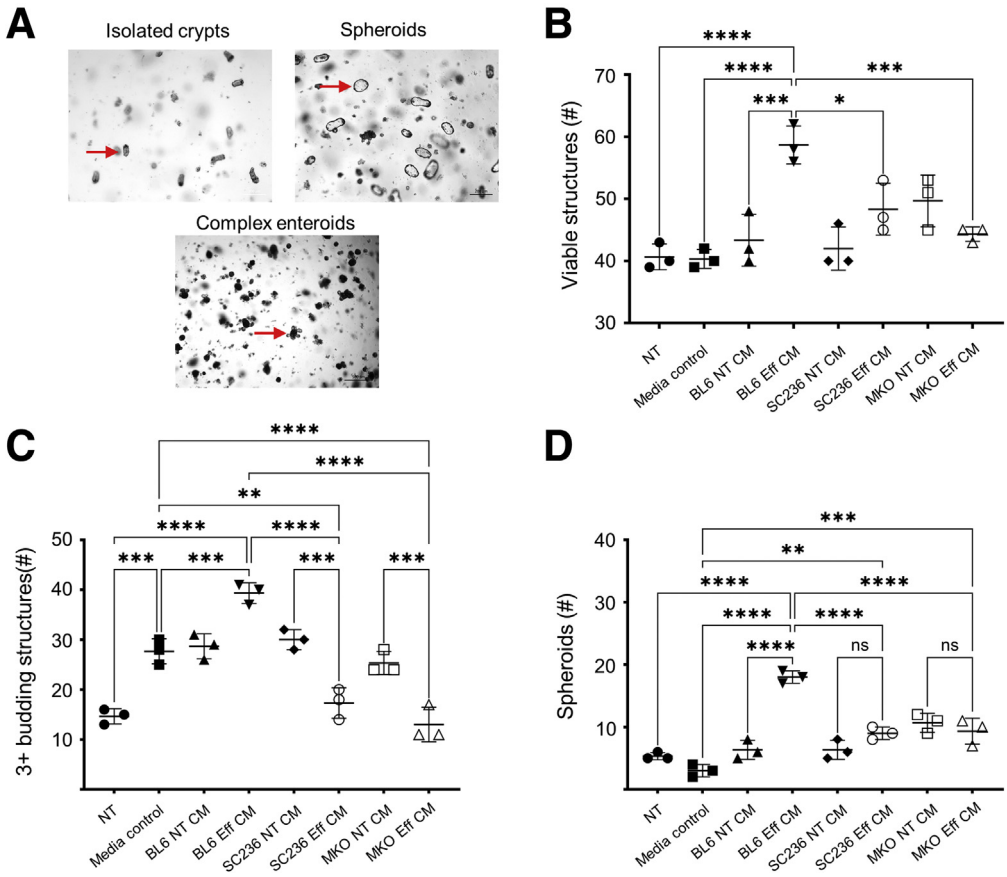

Figure 12. COX2-dependent products present in macrophage efferocytosis CM modulate induction of a tissue repair phenotype in small intestinal enteroids. (*A*) Crypts isolated from small intestinal epithelium and grown in Matrigel can form spheroids and complex multibudding enteroids (representative images). (*B–D*) Thioglycolate-elicited PMs were isolated from BL6 mice and cultured without (BL6) or with chronic COX2 inhibition (SC236). Thioglycolate-elicited PMs were also isolated from *Cox2* MKO mice. Each of the 3 types of PMs were then treated with apMPRO cells or vehicle; CM was collected from both apMPRO (Eff CM) and vehicle-treated (NT CM) PMs after 24 hours. The various CM were added to passaged enteroids derived from BL6 mice from time 0 hours following passage. The numbers of (*B*) viable structures at 72 hours, (*C*) complex 3+ budding enteroids and 72 hours, and (*D*) spheroids at 24 hours were determined as measures of epithelial restitution and repair. $^{*}P < .05$; $^{**}P < .01$; $^{***}P < .001$; $^{****}P < .0001$. One-way analysis of variance with Tukey's multiple comparisons test and adjusted *P* values. media control = macrophage media only; ns, not significant.

The mature enteroids were disrupted and recultured in fresh Matrigel, to model a tissue damage response. Immediately upon passage, enteroids were treated with 50% conditioned media from the 6 different PM cultures: BL6 ± apMPRO cells, SC236 ± apMPRO, and *Cox2* MKO ± apMPRO cells. These groups were compared with both NT and macrophage media–only control groups. The number of viable structures (Figure 12*B*) and 3+ budding structures (Figure 12*C*) were determined at 72 hours; the number of spheroids was determined at 24 hours (Figure 12*D*). BL6 efferocytic CM significantly increased all 3 measures compared with control media, while both *Cox2* MKO and chronic COX2 inhibition significantly suppressed these CM-dependent effects.

PGE2 induces spheroid formation in a PGE2-EP4 receptor dependent manner in enteroids grown under differentiation conditions.[41] Spheroids induced by PGE2 under these conditions are associated with epithelial restitution and express several markers characteristic of wound-associated epithelium (WAE) including *Cldn4*, *Dpcr2*, and *Daf2/Cd 55b*.[41] We had observed that the degree of spheroid formation following enteroid passage was correlated with the degree of enteroid disruption, and that PGE2 enhanced this effect.[44] Moreover, we had observed that an EP4 antagonist but not antagonists for EP1, EP2, or EP3 prevented PGE2-induced spheroid formation by crypts.[44] Independently, PGE2 increased additional enteroid measures of epithelial repair including the numbers of both viable and 3+ budding enteroids at 72 hours after passage (data available upon request).

Analysis by LC-MS/MS of the PM CM used in the experiment associated with Figure 12 demonstrated that apMPRO cell efferocytosis induced, in a COX2-dependent manner, PGE2, PGI2 (as measured by 6ketoPGF1α), and LXA4 (Figure 13*A–C*). These data suggested that CM from these macrophages would induce expression of WAE marker genes. The experiment associated with Figure 12 was repeated, using enteroid cultures grown from freshly

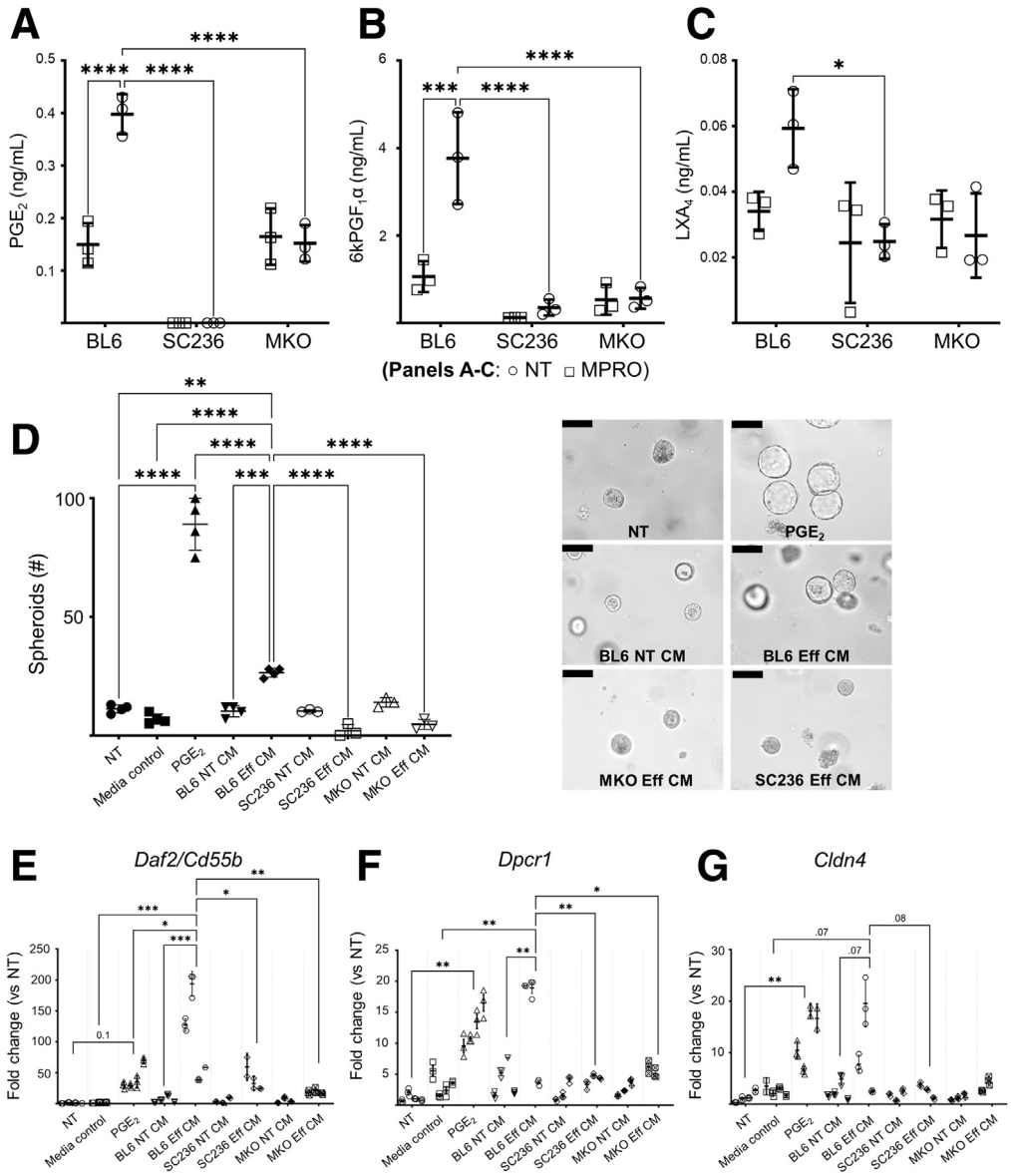

Figure 13. COX2 modulates the restitution signature induced in small intestinal enteroids by macrophage efferocytosis. (*A–C*) Thioglycolate-elicited PMs were isolated from BL6 mice and cultured without (BL6) or with chronic pharmacologic COX2 inhibition with SC236 (SC236). Thioglycolate-elicited PMs were also isolated from *Cox2* MKO. Each of the 3 types of PMs was treated with apMPRO cells (MPRO) or vehicle (NT), and CM was collected after 24 hours. Eicosanoid levels in the macrophage conditioned medias were determined by LC-MS/MS. All eicosanoids differentially increased by efferocytosis are represented, including PGE2, the PGI2 metabolite 6ketoPGF1α, and the inflammation resolving mediator LXA4. (*D*) Freshly isolated small intestinal crypts were grown in Matrigel as untreated control samples (NT) or treated with either 10 nM (approximately 3 ng/mL) PGE2 or macrophage media–only control (media control). Crypts were also treated with each of the 6 macrophage CMs associated with panels *A–C*. Eff CM indicates CM from macrophages treated with apMPRO cells; NT CM indicates CM from macrophages treated with vehicle. The induction of 24-hour spheroids was determined as a measure of restitution. Representative ×40 images with ×10 insets. Scale bars = 100 um. (*E–G*) Gene expression of the restitution-associated WAE markers *Daf2/Cd55b*, *Dpcr1*, and *Cld4* was determined for every group by qPCR. Three to 4 independent biological replicates were analyzed per condition. *$P < .05$; **$P < .01$; ***$P < .001$; ****$P < .0001$. (*A–C*) Two-way analysis of variance (ANOVA) with Sidak's multiple comparisons test and adjusted *P* values. (*D*) One-way ANOVA with Tukey's multiple comparisons test and adjusted *P* values. (*E–G*) Nested 1-way ANOVA with Holm-Sidak's multiple comparisons test and adjusted *P* values.

isolated crypts instead of passaged enteroids. PGE2 (10 nM) treatment was added for comparison. PGE2 strongly induced spheroid formation by 24 hours. BL6 efferocytic CM also significantly induced spheroid formation compared with control media, while both *Cox2* MKO and chronic COX2 inhibition significantly suppressed this effect (Figure 13*D*). Gene expression profiles of the enteroid cultures at 24 hours were analyzed (Figures 13*E–G*). Consistent with the prior report,[41] PGE2 significantly induced expression of the WAE markers *Cldn4* and *Dpcr2* and trended the induction of

Daf2/Cd55b. BL6 efferocytic CM significantly induced expression of the markers *Daf2/Cd55b* and *Dpcr2*, while trending *Cldn4* induction. Both *Cox2* MKO and COX2 inhibition blocked these inductive effects. Of note, BL6 efferocytic CM significantly increased *Daf2/Cd55b* expression when compared with PGE2 alone, suggesting that additional COX2-dependent factors beyond PGE2 were responsible for this increase.

Discussion

The role of macrophage COX2 in preserving intestinal immune homeostasis

We previously reported that *Cox2* MKO mice, but not control *Cox2* FLOX mice, developed TLR-dependent CD-like inflammation when their intestinal epithelial barrier was damaged by a cholate-containing diet.[5] Macrophage COX2 serves as check on TLR-dependent intestinal inflammation, in part by maintaining an appropriate balance of inflammatory and inflammation resolving mediators.[5] However, the results of the present investigation add importantly both to our understanding of the pathogenic mechanism of this model and to our understanding of the role of macrophage COX2 in preserving intestinal immune homeostasis.

Inflamed intestinal regions from *Cox2* MKO mice fed a CCHF diet exhibited high levels of both neutrophils and macrophages. In contrast, neutrophils were largely absent from comparable macrophage populations within COX2-expressing *Cox2* FLOX mice (Figure 1). This result suggested that the absence of COX2 within macrophages impairs their efferocytosis capacity; our subsequent in vitro studies support this hypothesis. The loss of COX2 suppresses the primary efferocytosis capacity of murine macrophages (Figures 3–6), and it further dysregulates the process by which primary efferocytosis programs an increase in efferocytosis capacity for secondary uptake of additional apoptotic cells (Figure 10).

Intestinal epithelium in inflammation-adjacent regions of *Cox2* MKO mice also exhibited considerably less proliferation than comparable regions in FLOX mice (Figure 11). This result further suggested that macrophage COX2 might modulate the effects of macrophage efferocytosis on intestinal epithelial restitution and repair. Again, our subsequent in vitro studies support this hypothesis. CM taken from macrophage cultures following efferocytosis of apoptotic neutrophils increased several measures of both intestinal epithelial restitution and repair, while loss of COX2 activity through either *Cox2* deletion or COX2 inhibition blocked these regenerative effects (Figures 12 and 13).

The overall picture that emerges of the pathogenic mechanism in the *Cox2* MKO model of IBD is of a set of complimentary dysregulations that appear to interlock into a multifaceted positive feedback loop (Figure 14). In this model, diet first disrupts epithelial barrier function and results in an influx of microbe-associated molecular patterns into the intestinal lamina propria.[5] Macrophages that lack COX2 respond to these inflammatory triggers with heightened inflammatory signaling including tumor necrosis factor α (TNFα) production (Figure 2). Higher levels of TNFα and other inflammatory signals recruit more neutrophils to the sites of response.[45] At the same time, macrophages that lack COX2 are less able to clear apoptotic neutrophils, and they further fail to produce anti-inflammatory signals like LXA4 that might suppress neutrophil recruitment (Figure 9). Apoptotic neutrophils that are not eliminated by macrophages undergo secondary necrosis and release the contents of intracellular granules, which can induce pathological epithelial damage.[46] Yet macrophages that lack COX2 are also less capable of promoting intestinal epithelial restitution and repair to counteract this damage. The damaged epithelium in turn admits even more microbe-associated molecular patterns to the LP while also directly triggering an inflammatory response. The cycle repeats and amplifies, overwhelming the capacity of the intestinal mucosal immune system to maintain homeostasis. Chronic pathological inflammation and tissue damage are the end results.

Aspects of this mechanism are consistent with emerging evidence that dysregulation of macrophage resolution function and reprogramming contributes to IBD.[14,47,48] First, several mouse models implicate efferocytosis in IBD,[49] and efferocytosis resulted in the overexpression of 41 susceptibility genes associated with IBD in intestinal macrophages.[17] Second, defects in the differentiation of inflammatory monocytes and immature macrophages into resolving macrophages appear to contribute to IBD,[14] with colonic macrophages in CD patients displaying abnormal inflammatory maturation.[50] Third, macrophage-dependent intestinal epithelial regeneration also appears to modulate IBD.[51]

Robustness of primary efferocytosis assay

Our basic efferocytosis assay produced a somewhat wide range of apMPRO or macrophage values at baseline and under COX2 deletion or inhibition (cf. Figure 3*A* and *B*). Across the 11 times we have performed this basic experiment, the baseline apMPRO-to-macrophage ratio for control macrophages ranged from approximately 0.6 to 3. (The average was 1.4, with SD = 0.9 and relative SD = 62%.) For the *Cox2* MKO and COX2 inhibited experimental groups, the apMPRO-to-macrophage ratio ranged from 0.5 to 1.5 (the average was 0.76, with SD = 0.44 and relative SD = 58%.) This degree of variance might call into question the robustness of the assay. We think that this variation is due at least in part to natural biological variation between PMs and BMDMs, between mice strains (BL6, $COX2f^{fl/fl}$, and $COX2^{fl/fl}$;$LysMCre^{+/-}$ mice), and across MPRO cultures. However, some of the interexperimental variation could also be due to technical noise that is introduced across experiments by the multiple cell counts, washes, treatments, and stains necessary to perform each assay. Nonetheless, in every case across these 11 studies, *Cox2* deletion (MKO) or COX2 pharmacologic inhibition (COX2i) significantly reduced the apMPRO-to-macrophage ratio. Moreover, across these experiments the levels of the MKO and COX2i groups ranged from 30% to 70% of control groups, with an average of 54%, an SD of 13%, and a relative SD of 24%.

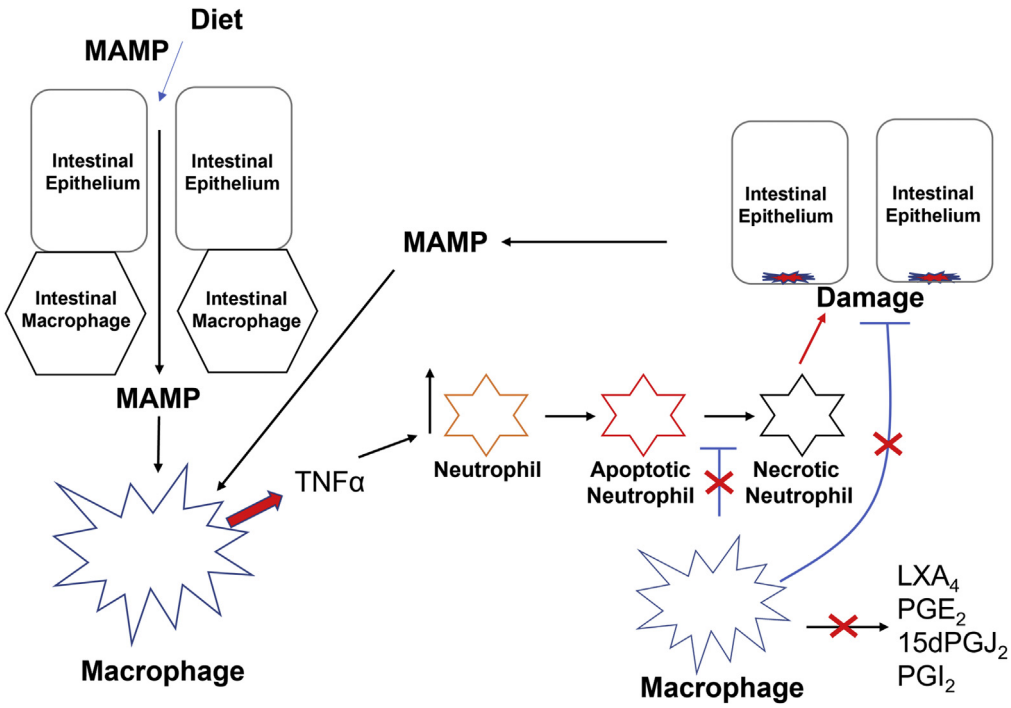

Figure 14. The pathogenic mechanism by which absence of myeloid COX2 produces CD-like inflammation in mice whose diet impairs their barrier function. A CCHF diet impairs barrier function and results in an influx of microbe-associated molecular patterns (MAMPs) into the lamina propria. Macrophages that lack COX2 overproduce inflammatory mediators including TNFα (Figure 2). TNFα recruits neutrophils, which undergo apoptosis. Macrophages that lack COX2 are unable to adequately clear apoptotic neutrophils (apNeutrophils) (Figures 2–5 and 7), which can undergo necrosis. Necrotic neutrophils damage intestinal epithelium. In the absence of COX2, macrophages that undergo efferocytosis fail to secrete anti-inflammatory and inflammation-resolving lipid mediators (Figure 6), and they are inadequate in promoting epithelial restitution and repair (Figures 9 and 10). The subsequent necrotic neutrophil-damaged epithelium results in even more influx of MAMPs, amplifying the cycle. Red symbols indicate the effects of loss of macrophage COX2.

Determination of the effect of *Cox2* MKO and COX2i on the efferocytosis capacity of PMs and BMDMs was thus largely immune to the presence of interexperimental variance. At this second-order level, the assay was thus comparatively robust: it yielded the same result in every study regardless of any possible technical variation.

Modulation of the primary efferocytosis capacity of mouse macrophage

Our results partially elucidate the mechanism by which COX2 loss reduces the primary efferocytosis capacity of mouse macrophages. COX2 modulated the binding capacity of primary macrophages for apoptotic neutrophils (Figure 5), and it also modulated expression of genes involved in apoptotic cell binding (Figure 8). These results suggest that COX2 affects the levels of proteins involved in apoptotic cell binding—reducing apoptotic cell binding capacity and consequently reducing efferocytosis capacity. The failure of COX2-inhibited macrophages to significantly reduce efferocytic efficiency (Figure 6*C*) is consistent with these results.

High-dose LPS also reduced the expression of genes involved in apoptotic cell binding (Figure 8), and loss of COX2 activity reduced the efferocytosis index of primary macrophages to a level comparable to high-dose LPS (Figure 6). These results strengthen the correlation between overall efferocytosis capacity, and the expression levels of genes involved in apoptotic cell binding. They also suggest a further explanation for the effect of COX2 on efferocytosis.

High-dose LPS induces M1 polarization, and M1 macrophages have less efferocytosis capacity than M2/M2c macrophages.[20] Likewise, there is evidence that COX2 can modulate macrophage polarization phenotype, thereby modulating efferocytosis capacity.[7,8,52–54] Altogether, these reports indicate that COX2 activity during both differentiation and polarization can potentiate alternatively activated phenotypes and that the COX2 loss can promote classical activation. Consistent with these reports, we detected COX2-dependent prostanoids during the differentiation of BMDMs (Figure 7). We also observed that absence of COX2 activity during differentiation and M2-specific BMDM polarization enhanced expression of *iNos* while reducing expression of *Ym1* (Figure 7). These data suggest that COX2 loss may reduce primary efferocytosis capacity in both PMs and BMDMs by biasing these macrophages toward a classically activated M1 state.

Efferocytosis-dependent eicosanoidomics

There exist reports of individual eicosanoids produced by efferocytic macrophages.[29,55–59] There are also reports of

eicosanoid lipidomic (eicosanoidomic) profiles associated both with classically and with alternatively activated macrophages.[60,61] However, our LC-MS/MS examination of the levels of efferocytosis-dependent eicosanoids secreted by elicited murine PMs across 32 hours (Figure 9) is the only example we are aware of for any eicosanoidomic profiles of efferocytic macrophages over the time course associated with efferocytosis-dependent macrophage reprogramming.

Macrophage efferocytosis of apoptotic neutrophils significantly increased, in a time-dependent manner, the secreted levels of several eicosanoids associated with resolution. PGE2 can promote intestinal immune tolerance and can enhance the anti-inflammatory function of mouse intestinal macrophages,[62] while PGD2 can signal through its receptor DP1 to promote M2 polarization.[63] Both the PGD2-deriviative 15d-PGJ2 and LXA4 can increase macrophage efferocytosis and efferocytosis capacity.[31,64]

LXA4 is formed from arachidonic acid by enzymatic oxygenation at the 15th carbon and fourth/fifth carbons. LXA4 can be produced by macrophages in a COX2-dependent manner; COX2-derived 15HETE is conjugated to LXA4 by ALOX5.[9] LXA4 can also be produced by the combined actions of both ALOX5 and ALOX15. COX2 inhibition significantly suppressed LXA4 levels (Figure 9*D*), suggesting that COX2 substantially mediates efferocytosis-dependent LXA4 production. Apoptotic cell binding alone, without macrophage ingestion, is sufficient to induce LXA4 (Figure 9*D*). This last observation is consistent with reports that activation of the indirect PS receptor MERTK is sufficient to trigger LXA4 production in macrophages.[57,58]

Efferocytosis-dependent intestinal epithelial repair capacity

The intestinal epithelium consists of a single layer of epithelial cells that separate the intestinal luminal contents from the immune cells, vasculature, and structural cells of the LP. During homeostasis, epithelial cells are constantly replaced from a population of self-renewing proliferative cells (intestinal stem cells) that reside at the base of crypts.[65,66] When the intestinal epithelium is injured or damaged, the barrier must be quickly reestablished, to prevent exposure to luminal antigens and invasion of intestinal microorganisms. The intestinal epithelium undergoes repair in 2 separate steps, epithelial restitution and epithelial repair. During epithelial restitution, a transient class of specialized epithelial repair cells of atypical differentiation state forms within hours. These WAE cells migrate over wounds and damaged epithelium and seek to reestablish the epithelial barrier.[41,67–69] During epithelial repair, the intestinal stem cells proliferate and differentiate into progenitors more rapidly than in undamaged epithelium, and damaged crypts either regenerate or are replaced by budding or fission from neighboring crypts.[70,71]

The small intestinal enteroid assays described here provide some measure of both epithelial restitution and epithelial repair. WAE cells differentially express the markers *Cldn4*,[71] *Dpcr1*,[41] and *Cd55* or *Daf2*.[41] WAE cells are also associated with spheroids that develop quickly following passage of intestinal organoid cultures into media depleted of growth factors including WNT.[41] To measure restitution, we determined the degree of spheroid production in partially depleted medium at 24 hours following either enteroid passage or crypt culture and also analyzed *Cldn4*, *Dpcr1*, and *Cd55/Daf2* gene expression. To assess epithelial repair, we determined both enteroid budding as a measure of crypt regeneration and the percentage of passaged elements or isolated crypts that gave rise to viable enteroids at 72 hours. We assumed throughout that both crypt isolation and enteroid passage constituted types of mechanical epithelial damage.

PGE2 is a key mediator of WAE cell expansion in response to epithelial wounding, enhancing WAE gene expression while inducing EP4 receptor–dependent spheroids upon passage of small intestinal epithelial organoids into depleted media containing only EGF.[41] Our results are consistent with observations from this report, and we thus suggest that PGE2 contributes to the restitution and repair responses we observed. Nonetheless, it is important to emphasize that PGE2 is not the only contributing factor to the observed response. BL6 efferocytosis CM contained approximately 10-fold less PGE2 than did our PGE2-positive control media (Figure 13*A*). Nonetheless, BL6 CM induced significantly higher levels of *Daf2/Cd55b* and comparable levels of *Dpcr2* and *Cldn4* compared with PGE2 alone. These results suggest that there exists at least some additional COX2 dependent factor, other than PGE2, that is present in efferocytosis CM and that also affects intestinal epithelial restitution and repair. Hepatocyte growth factor, produced by macrophages in a COX2-dependent manner upon exposure to apoptotic cells, is a possible candidate.[29] LXA4 and a PGI2 degradation product 6ketePGF1α are also present in in BL6 efferocytosis CM (Figure 13*B* and *C*)[72] and may contribute to intestinal epithelial restitution and repair in our assays.[73] In future studies, we will try to identify additional COX2-dependent factors that mediate the effect of macrophage efferocytosis on intestinal epithelial repair, and further clarify the role of PGE2.

Materials and Methods

Mice

The procedures for all animal experiments were approved by the UCLA Animal Research Committee, and all experiments were carried out in accordance with the approved guidelines. *Cox2*$^{fl/fl}$;LysMCre$^{+/-}$ (*Cox2* MKO) mice, *Cox2*$^{fl/fl}$; LysMCre$^{-/-}$ (FLOX), and *Cox2*$^{luc/luc}$ (*Cox2* KO) mice were bred and genotyped as previously described.[5,74] C57Bl/6J (BL6) mice were from the Jackson Laboratory (Bar Harbor, ME). All mice used in experiments were approximately 4–6 months old. Equal numbers of male and female mice were used when possible. For studies involving CCHF diet (TD.88051; Envigo, Indianapolis, IN), mice were fed for either 2 weeks or 10 weeks as indicated.

Primary Macrophages

Thioglycolate-elicited PMs and BMDMs were isolated and maintained as previously described.[5] Macrophages

differentiated from bone marrow derived monocytes in macrophage CSF were subcultured on day 6 and polarized on day 8. BMDMs were polarized with 20 ng/mL IL-10, 20 ng/mL IL-4, 10 ng/mL LPS, or 100 ng/mL LPS, or were left without further treatment. All BMDM experiments were performed on day 10 unless otherwise specified. All PM studies were conducted on day 7 unless otherwise specified. Macrophage COX2 was inhibited with 250 nM SC236 (Cayman 10004219; Cayman Chemical, Ann Arbor, MI) either chronically from primary cell isolation or acutely from 1 hour prior to the study in question. For continuous inhibition, SC236 was refreshed with every media change. Actin filament polymerization and apoptotic cell engulfment were inhibited with 5 μM cytochalasin D (PHZ1063; Life Technologies, Carlsbad, CA).

Murine MPRO Neutrophils

MPRO cells (#11422; ATCC, Manassas, VA) were maintained in accord with the ATCC protocol. Growth medium consisted of Iscove's modified Dulbecco's medium with 4 mM L-glutamine adjusted to contain 1.5 g/L sodium bicarbonate containing 10 ng/mL murine granulocyte macrophage CSF (murine granulocyte-macrophage CSF, # 315-03; PeproTech, Rocky Hill, NJ) and 20% heat-inactivated horse serum. Apoptosis was induced in MPRO cells with 1 μM staurosporine (#20056; Abcam, Cambridge, United Kingdom) for 4 hours at 37°C.[20] ApMPRO cells were fluorescently stained with Cell Proliferation Dye eFluor 450 (65-0842-85; Invitrogen, Waltham, MA) per the manufacturer's protocol. This fluorescent dye binds to any cellular proteins containing primary amines, thereby labeling the entire cell violet (ex 405/em 450).

Efferocytosis Capacity

Efferocytosis capacity was determined as the number of cell internalized or membrane bound apMPRO neutrophils per primary macrophage at 60 minutes. Our protocol was adapted from Evans et al.[20] In brief, apMPRO cells were added to primary macrophages grown in glass bottom 12 well plates (Cellvis, Burlington, Canada; p12.1.5H-N) at 1×10^6 apMPRO cells per well. The apMPRO cells were either centrifuged at 300 *g* for 1 minute, or allowed to settle at room temperature for 10 minutes, in order to bring the apMPRO cells into contact with the macrophages. After 1 hour at 37°C, primary macrophages were washed 3× with phosphate-buffered saline (PBS). Macrophage nuclei were stained with Nuclear Green DCS1 (17550; AAT Bioquest, Sunnyvale, CA), while macrophage cell membrane was stained with wheat germ agglutinin Texas red (Invitrogen; W21405). Cells were fixed using 4% paraformaldehyde in PBS for 15 minutes. Cells were imaged on a Leica DMi8 (Leica, Wetzlar, Germany) inverted fluorescent microscope as further described herein.

Phagocytosis Capacity

Phagocytosis capacity for opsonized apMPRO was determined as for efferocytosis capacity, except that apMPRO cells were opsonized in mouse serum for 30 minutes at 37°C prior to application.

Efferocytic Index and Efficiency

Both efferocytic index and efficiency were determined using 2 color synthetic apoptotic cell targets in accord with published protocols.[20] In brief, these synthetic targets consisted of 2.5 um silica beads (Bangs Labs, Fishers, IN; SS05000) coated with 80% PC, 20% PS, 0.1% PE-rhodamine, and 0.1% PE-biotin (all from Avanti Polar Lipids, Alabaster, AL). Primary macrophages were grown in confocal compatible dishes. Concentration-optimized beads were added to the macrophages, spun at 300 *g* for 1 minute, and allowed to bind at 37°C for 10 minutes, and then the cells were washed of remaining beads. After an additional 45 minutes, cells were washed 3× with PBS and stained with streptavidin AF 647 (Invitrogen; S32357) for 4 minutes. After washing, cells were fixed in 4% paraformaldehyde and further stained with membrane dye wheat germ agglutinin (Alexa Fluor 488 Conjugate; Invitrogen; #W11261) and nuclear dye DAPI (Invitrogen; #D1306). Cells were imaged on a Zeiss confocal microscope (Zeiss, Oberkochen, Germany) as further described herein. Efferocytic index was defined as the number of single color rhodamine positive beads per macrophage. Efferocytic efficiency was defined as the number of single-color rhodamine-positive beads as a percent of both single-color rhodamine-positive beads and double-color rhodamine and far red–positive beads.

Flow Cytometry

Flow cytometry analysis was utilized to determine PM viability. Cells were detached from tissue culture dishes by gentle scraping in 500 μL of Accutase (Innovative Cell Technologies, San Diego, CA) and then washed twice with fluorescence-activated cell sorting buffer (PBS + 2% [v/v] FBS). Following washes, cells were suspended in 1 μg mL^{-1} DAPI and analyzed on flow cytometer (Attune NxT; Thermo Fisher Scientific, Waltham, MA). FlowJo X10.0.7r2 (FlowJo, Ashland, OR) was used to quantify the DAPI exclusion of live cells.

Histology

Ileo-ceco-colic regions from Cox2$^{fl/fl}$; LysMCre$^{+/-}$ and COX2$^{fl/fl}$ mice were fixed in formaldehyde and paraffin embedded for sectioning. The sections were de-paraffinized in xylene, rehydrated, and treated with citrate buffer for antigen retrieval. Triton X-100 (0.2%) was used for permeabilization. Slides were stained with hematoxylin and eosin for determination of total area of inflammation within each cross-section. Additional slides were probed with primary antibodies against LY6G (BioLegend, San Diego, CA; #127601), F4/80 (Cell Signaling Technology, Danvers, MA; #D2S9R), KI67 (Cell Signaling Technology; #D3B8), and CDH1 (R&D Systems, Minneapolis, MN; #AF748) overnight at 1:200 in blocking buffer. After washing with 1× PBS, the corresponding secondary antibodies (goat AF568 [Abcam] #ab175704; rabbit AF647 [Abcam] #ab150063; rat AF647

[Abcam] #ab150155; rabbit AF488 [Invitrogen] #A32790) along with DAPI and then mounted with glass coverslips using mounting media (AAT Bioquest; #20009) for confocal imaging.

Microscopy

Confocal microscopy. Confocal imaging was performed on a Zeiss LSM 900 confocal microscope equipped with 405 nm, 488 nm, 561 nm, and 640 nm laser lines. For fixed cells, images were acquired using a Plan-Apochromat ×20/0.8 M27 objective and Airyscan 2 GaAsP-PMT detector. Identical laser intensity settings were applied to all samples and Z-stacks were performed to acquire 11-μm sections. After acquisition, a maximum intensity projection of the Z-stack was applied using ZEN Blue 3.0 software (Zeiss). Intestine imaging was perform using a Plan-Apochromat 10×/0.45 M27 objective. Z-stack tile scans (3 × 3 or 28 × 28) were acquired to capture the full thickness of the slice and large regions of the intestinal tissue. After acquisition, tiles were stitched and a maximum intensity projection of the Z-stack was applied using ZEN Blue 3.0 software.

Inverted fluorescence microscopy. Imaging was performed on a Leica DMi8 inverted fluorescent microscope equipped with DAPI, rhodamine, and FITC fluorescent filters and controlled by Leica LAS X software. Optimized settings were applied evenly across all samples, and pictures were taken with a Leica DFC7000T camera. For all imaging studies, multiple random fields per condition were taken.

Image Analysis

Nuclei, apMPRO cells, and PC-PS beads were counted in ImageJ (National Institutes of Health, Bethesda, MD; v1.53k) by analysis of the appropriate fluorescent images using the Analyze Particles function following color thresholding and settings optimization. F4/80 and LY6G were determined in FIJI (ImageJ) by measuring signal intensity in approximately 20 (200 μm)^2 regions of interest within higher magnification tiled micrographs of each cross-section. Both the areas to tile and the subsequent ROI were selected on the basis of comparable F4/80 intensity across samples. For KI67, regions of interest were traced in FIJI by cursor around the boundary of every crypt that was longitudinally sectioned on axis; and KI67 was determined as % positive area within each region of interest after color thresholding.

RNA isolation and qPCR analysis of macrophages

For RNA isolation, 4 × 10^5 BMDMs or PMs were seeded into 12-well plates and polarized or treated as detailed previously. Following polarization, RNA was isolated using the Zymo Research Quick-RNA Microprep kit. Complementary DNA was synthesized with the high-capacity complementary DNA reverse transcription kit (Applied Biosystems, Waltham, MA). Reverse-transcriptase qPCR assay was performed using PowerUp SYBR Green qPCR Master Mix kit (Applied Biosystems) and QuantStudio system (Applied Biosystems). Data were analyzed using the comparative Ct method with 36b4 as the reference gene. For TNFα, the primer sequences F: TGCCTATGTCTCAGCCTCTTC and R: GAGGCCATTTGGGAACTTCT were used.

Efferocytosis genes

Primer sequences for efferocytosis specific genes were selected from validated sequences presented in PrimerBank (https://pga.mgh.harvard.edu/primerbank/) and employed in at least 1 peer reviewed study. Primer sequences: *Stab1* F TCTGAGTATCAATGCCAGCC; R ATTTGACCTTGAGGACCCTC. *Tim3* F TCAGGTCTTACCCTCAACTGTG; R GGCATTCTTACCAACCTCAAACA. *Gas6* FAGGTCTGCCACAACAAACCA; R GCGTAGTCTAATCACGGGGG. *Mfge8* F ATATGGGTTTCATGGGCTTG; R GAGGCTGTAAGCCACCTTGA. *Pros1* F GCACAGTGCCCTTTGCCT; R CAAATACCACAATATCCTGAGACGTT. *Mertk* F GCTCGAAACTGCATGTTGCGGGAT; R CTCGGTCCGCCAGGCTCTCG. *Axl* F ATGCCAGTC AAGTGGATTGCT; R CACACATCGCTCTTGCTGGT. *Elmo1* F ACTTTGGTCTCACTTGTAGCAG; R CAGTGTGATAGAGGGATTGGTC. *Dock2* F TCGGTGGAGAACTTTGTGAG; R ACGGTTGTCTTTGCTCTCATC. *Rac1* F ATAGGCCCAGATTCACTGGTT; R GAGACGGAGCTGTTGGTAAAA.

Determination of efferocytosis-dependent eicosanoids by LC-MS/MS

Mouse primary macrophages were plated into 6-well dishes at 1 × 10^6 cells/well and equilibrated to lipoprotein deficient FBS for 1–2 hours. Macrophages were treated with apMPRO cells as previous. After 1 hour, unbound apMPRO cells were washed off. Media were collected across 32 hours and frozen at −80°C prior to preparation and analysis. Eicosanoids were isolated from media and analyzed by LC-MS/MS as previously described.[5] In brief, 40 separate eicosanoids and docosanoids from COX and LOX pathways were measured along with 20 matching or class specific heavy labeled internal standards using a SCIEX 5500 QTrap (AB Sciex, Framingham, MA) instrument and Agilent 1290 UHPLC system (Agilent, Santa Clara, CA) controlled by SCIEX Analyst 1.6. Analysis was performed with SCIEX Multiquant software.

AnV inhibition of efferocytosis

Apoptotic neutrophils with and without labeling by Cell Proliferation Dye were combined with vehicle or 500 ng/mL murine recombinant annexin V (Kingfisher Biotech, St Paul, MN; RP1685M). PMs were treated with labeled apMPRO ± AnV for determination of efferocytosis by fluorescent microscopy. For determination of eicosanoids released over 24 hours, PMs were treated with unlabeled apMPRO ± AnV.

Secondary efferocytosis and phagocytosis capacities

Primary macrophages were grown in 12-well plates. Media were changed to OptiMEM (Gibco, Gaithersburg, MD) + 0.2% BSA, and treated with apoptotic but unstained MPRO cells (1 × 10^6 apMPRO cells/well). After 1 hour, unbound apMPRO cells were washed off and OptiMEM + 0.2% BSA was replenished. After 24 hours, efferocytosis

capacity was determined by adding labeled apMPRO cells, as previous. For secondary phagocytosis capacity, the same protocol was followed, except that apMPRO cells were opsonized in mouse serum for 30 minutes at 37°C prior to addition to PMs.

Enteroids

Small intestinal enteroids were grown in Matrigel from isolated small intestinal crypts or upon passage of existing enteroids as previously described.[75,76] In brief, crypts or passaged enteroids were seeded at approximately 150 structures per 25 μl Matrigel per well. Culture medium consisted of Advanced Dulbecco's modified Eagle Medium/F12 containing 50 ng/mL EGF, 100 ng/mL Noggin, 500 ng/mL human R-spondin 1, 1 mM N-acetylcysteine, and 1% N2 supplement and B27 supplement.

Macrophage CM and enteroid repair and restitution assay

Primary macrophages were equilibrated with lipoprotein-deficient FBS and treated with unstained apMPRO cells as previous. Media were sampled across 24–32 hours and stored at −80°C prior to use. Eicosanoid levels were determined by LC-MS/MS as previous. CM or control media was diluted 1:2 in 2× enteroid growth media. Enteroid cultures were monitored over 24–72 hours. Spheroid and viable structure percentages, and the number of 3+ budding enteroids, were determined by analyzing bright-field microscope images that covered the entirety of each Matrigel culture. RNA was isolated and analyzed at 24 hours. Spheroid percentage was determined at 24 hours. Viable structure percentage and 3+ budding structure number were determined at 72 hours.

RNA isolation and qPCR analysis of enteroids

RNA was isolated from enteroids using a PureLink RNA Mini Kit (Invitrogen). Following RNA isolation, qPCR was performed using a 1 step-TaqMan assay (Life Technologies, Carlsbad, CA; #43928938) in a real-time thermocycler (Applied Biosystems; 7500). The results obtained for each individual gene were normalized to GAPDH; *Cldn4* Catalog number: 4448892 (Assay ID: Mm01196224_s1), *Daf2* Catalog number: 4448892 (Assay ID: Mm00432792_g1), *Dpcr1* Catalog number: 4448892 (Assay ID: Mm02600627_g1), GAPDH Catalog number: 4448892 (Assay ID: Mn99999915_g1).

Statistics

For lipidomic analyses, false discovery rate corrections were performed by application of the Benjamini-Hochberg procedure to P values determined for each analyte by 1-way analysis of variance, with false discovery rate controlled at level $\alpha = 0.05$. For each analyte within a data set deemed a discovery or significant, post hoc analyses consisted 2-way analysis of variance with Tukey's multiple comparisons test. Heatmap was generated in ClustVis; rows were clustered using correlation distance and average linkage.[77] For all other multiple comparisons, 1- or 2-way analysis of variance was followed by Tukey's, Sidak's, or Holm-Sidak's multiple comparisons tests (see figure legends for application details) For comparisons involving 1 independent variable with 2 groups, we performed Student's t tests; for studies consisting of more than 1 Student's t tests, we performed Holm-Sidak's multiple comparisons test. In all cases of multiple comparisons and tests, we adjusted P values in accord with the appropriate correction. Statistical significance was set at $P < .05$ with respect to final (adjusted) P values. Variation is reported as SD. All experiments were conducted in at least biological triplicate and performed multiple times.

References

1. Xavier RJ, Podolsky DK. Unravelling the pathogenesis of inflammatory bowel disease. Nature 2007;448:427–434.
2. Liu JZ, van Sommeren S, Huang H, Ng SC, Alberts R, Takahashi A, Ripke S, Lee JC, Jostins L, Shah T, Abedian S, Cheon JH, Cho J, Daryani NE, Franke L, Fuyuno Y, Hart A, Juyal RC, Juyal G, Kim WH, Morris AP, Poustchi H, Newman WG, Midha V, Orchard TR, Vahedi H, Sood A, Sung JJY, Malekzadeh R, Westra H-J, Yamazaki K, Yang S-Koll, International Multiple Sclerosis Genetics Consortium; , International IBD Genetics Consortium, Barrett JC, Franke A, Alizadeh BZ, Parkes M, B K T, Daly MJ, Kubo M, Anderson CA. Weersma RK. Association analyses identify 38 susceptibility loci for inflammatory bowel disease and highlight shared genetic risk across populations. Nat Genet 2015;47:979.
3. Lee JC, Biasci D, Roberts R, Gearry RB, Mansfield JC, Ahmad T, Prescott NJ, Satsangi J, Wilson DC, Jostins L, Anderson CA, Consortium UIG, Traherne JA, Lyons PA, Parkes M, Smith KGC. Genome-wide association study identifies distinct genetic contributions to prognosis and susceptibility in Crohn's disease. Nat Genet 2017;49:262.
4. Rouzer CA, Marnett LJ. Cyclooxygenases: structural and functional insights. J Lipid Res 2009;50 Suppl(Suppl): S29–S34.
5. Meriwether D, Sulaiman D, Volpe C, Dorfman A, Grijalva V, Dorreh N, Solorzano-Vargas RS, Wang J, O'Connor E, Papesh J, Larauche M, Trost H, Palgunachari MN, Anantharamaiah GM, Herschman HR, Martin MG, Fogelman AM, Reddy ST. Apolipoprotein A-I mimetics mitigate intestinal inflammation in COX2-dependent inflammatory bowel disease model. J Clin Invest 2019;130:3670–3685.
6. Gitlin JM, Loftin CD. Cyclooxygenase-2 inhibition increases lipopolysaccharide-induced atherosclerosis in mice. Cardiovasc Res 2009;81:400–407.
7. Na Y-R, Yoon Y-N, Son D-I, Seok S-H. Cyclooxygenase-2 inhibition blocks M2 macrophage differentiation and suppresses metastasis in murine breast cancer model. PLoS One 2013;8:e63451.
8. Na YR, Yoon YN, Son D, Jung D, Gu GJ, Seok SH. Consistent inhibition of cyclooxygenase drives macrophages towards the inflammatory phenotype. PLoS One 2015;10:e0118203.

9. Norris PC, Gosselin D, Reichart D, Glass CK, Dennis EA. Phospholipase A2 regulates eicosanoid class switching during inflammasome activation. Proc Natl Acad Sci U S A 2014;111:12746–12751.
10. Romano M, Cianci E, Simiele F, Recchiuti A. Lipoxins and aspirin-triggered lipoxins in resolution of inflammation. Eur J Pharmacol 2015;760:49–63.
11. Serhan CN, Chiang N. Resolution phase lipid mediators of inflammation: agonists of resolution. Curr Opin Pharmacol 2013;13:632–640.
12. Fox S, Leitch AE, Duffin R, Haslett C, Rossi AG. Neutrophil apoptosis: relevance to the innate immune response and inflammatory disease. J Innate Immun 2010;2:216–227.
13. Elliott MR, Koster KM, Murphy PS. Efferocytosis signaling in the regulation of macrophage inflammatory responses. J Immunol 2017;198:1387–1394.
14. Na YR, Stakenborg M, Seok SH, Matteoli G. Macrophages in intestinal inflammation and resolution: a potential therapeutic target in IBD. Nat Rev Gastroenterol Hepatol 2019;16:531–543.
15. Gordon S, Plüddemann A. Macrophage clearance of apoptotic cells: a critical assessment. Front Immunol 2018;9:127.
16. A-Gonzalez N, Bensinger SJ, Hong C, Beceiro S, Bradley MN, Zelcer N, Deniz J, Ramirez C, Díaz M, Gallardo G, de Galarreta CR, Salazar J, Lopez F, Edwards P, Parks J, Andujar M, Tontonoz P, Castrillo A. Apoptotic cells promote their own clearance and immune tolerance through activation of the nuclear receptor LXR. Immunity 2009;31:245–258.
17. Cummings RJ, Barbet G, Bongers G, Hartmann BM, Gettler K, Muniz L, Furtado GC, Cho J, Lira SA, Blander JM. Different tissue phagocytes sample apoptotic cells to direct distinct homeostasis programs. Nature 2016;539:565–569.
18. Baillie JK, Arner E, Daub C, De Hoon M, Itoh M, Kawaji H, Lassmann T, Carninci P, Forrest ARR, Hayashizaki Y, Consortium F, Faulkner GJ, Wells CA, Rehli M, Pavli P, Summers KM, Hume DA. Analysis of the human monocyte-derived macrophage transcriptome and response to lipopolysaccharide provides new insights into genetic aetiology of inflammatory bowel disease. PLoS Genet 2017;13:e1006641.
19. Bernardo D, Marin AC, Fernandez-Tome S, Montalban-Arques A, Carrasco A, Tristan E, Ortega-Moreno L, Mora-Gutierrez I, Diaz-Guerra A, Caminero-Fernandez R, Miranda P, Casals F, Caldas M, Jimenez M, Casabona S, De la Morena F, Esteve M, Santander C, Chaparro M, Gisbert JP. Human intestinal pro-inflammatory CD11c(high)CCR2(+)CX3CR1(+) macrophages, but not their tolerogenic CD11c(-)CCR2(-)CX3CR1(-) counterparts, are expanded in inflammatory bowel disease. Mucosal Immunol 2018;11:1114–1126.
20. Evans AL, Blackburn JW, Yin C, Heit B. Quantitative efferocytosis assays. Methods Mol Biol 2017;1519:25–41.
21. Lawson ND, Krause DS, Berliner N. Normal neutrophil differentiation and secondary granule gene expression in the EML and MPRO cell lines. Exp Hematol 1998; 26:1178–1185.
22. Cassado AdA, D'Império Lima MR, Bortoluci KR. Revisiting mouse peritoneal macrophages: heterogeneity, development, and function. Front Immunol 2015; 6:225.
23. Zizzo G, Hilliard BA, Monestier M, Cohen PL. Efficient clearance of early apoptotic cells by human macrophages requires M2c polarization and MerTK induction. J Immunol 2012;189:3508–3520.
24. Hobbs S, Reynoso M, Geddis AV, Mitrophanov AY, Matheny RW Jr. LPS-stimulated NF-kappaB p65 dynamic response marks the initiation of TNF expression and transition to IL-10 expression in RAW 264.7 macrophages. Physiol Rep 2018;6:e13914.
25. Zhao Y-L, Tian P-X, Han F, Zheng J, Xia X-X, Xue W-J, Ding X-M, Ding C-G. Comparison of the characteristics of macrophages derived from murine spleen, peritoneal cavity, and bone marrow. J Zhejiang Univ Sci B 2017; 18:1055–1063.
26. Doran AC, Yurdagul A, Tabas I. Efferocytosis in health and disease. Nat Rev Immunol 2020;20:254–267.
27. Wang Y, Subramanian M, Yurdagul A Jr, Barbosa-Lorenzi VC, Cai B, de Juan-Sanz J, Ryan TA, Nomura M, Maxfield FR, Tabas I. Mitochondrial fission promotes the continued clearance of apoptotic cells by macrophages. Cell 2017;171:331–345.e22.
28. Jablonski KA, Amici SA, Webb LM, Ruiz-Rosado JdD, Popovich PG, Partida-Sanchez S, Guerau-de-Arellano M. Novel markers to delineate murine M1 and M2 macrophages. PLoS One 2015;10:e0145342.
29. Byun JY, Youn YS, Lee YJ, Choi YH, Woo SY, Kang JL. Interaction of apoptotic cells with macrophages upregulates COX-2/PGE2 and HGF expression via a positive feedback loop. Mediators Inflamm 2014;2014:463524.
30. Yoshida S, Minematsu N, Chubachi S, Nakamura H, Miyazaki M, Tsuduki K, Takahashi S, Miyasho T, Iwabuchi T, Takamiya R, Tateno H, Mouded M, Shapiro SD, Asano K, Betsuyaku T. Annexin V decreases PS-mediated macrophage efferocytosis and deteriorates elastase-induced pulmonary emphysema in mice. Am J Physiol Lung Cell Mol Physiol 2012;303:L852–L860.
31. Godson C, Mitchell S, Harvey K, Petasis NA, Hogg N, Brady HR. Cutting edge: lipoxins rapidly stimulate nonphlogistic phagocytosis of apoptotic neutrophils by monocyte-derived macrophages. J Immunol 2000; 164:1663–1667.
32. Frasch SC, Fernandez-Boyanapalli RF, Berry KZ, Leslie CC, Bonventre JV, Murphy RC, Henson PM, Bratton DL. Signaling via macrophage G2A enhances efferocytosis of dying neutrophils by augmentation of Rac activity. J Biol Chem 2011;286:12108–12122.
33. Kim W, Jang J-H, Zhong X, Seo H, Surh Y-J. 15-Deoxy-△(12,14)-prostaglandin J(2) promotes resolution of experimentally induced colitis. Front Immunol 2021; 12:615803.
34. Na YR, Jung D, Yoon BR, Lee WW, Seok SH. Endogenous prostaglandin E2 potentiates anti-inflammatory phenotype of macrophage through the CREB-C/EBP-β cascade. Eur J Immunol 2015;45:2661–2671.
35. Niederstaetter L, Neuditschko B, Brunmair J, Janker L, Bileck A, Del Favero G, Gerner C. Eicosanoid content in

fetal calf serum accounts for reproducibility challenges in cell culture. Biomolecules 2021;11:113.
36. Bailey JD, Shaw A, McNeill E, Nicol T, Diotallevi M, Chuaiphichai S, Patel J, Hale A, Channon KM, Crabtree MJ. Isolation and culture of murine bone marrow-derived macrophages for nitric oxide and redox biology. Nitric Oxide 2020;100–101:17–29.
37. Hart SP, Smith JR, Dransfield I. Phagocytosis of opsonized apoptotic cells: roles for 'old-fashioned' receptors for antibody and complement. Clin Exp Immunol 2004;135:181–185.
38. Wallach TE, Bayrer JR. Intestinal organoids: new frontiers in the study of intestinal disease and physiology. J Pediatr Gastroenterol Nutr 2017;64:180–185.
39. Gregorieff A, Liu Y, Inanlou MR, Khomchuk Y, Wrana JL. Yap-dependent reprogramming of Lgr5+ stem cells drives intestinal regeneration and cancer. Nature 2015; 526:715–718.
40. Oudhoff MJ, Braam MJS, Freeman SA, Wong D, Rattray DG, Wang J, Antignano F, Snyder K, Refaeli I, Hughes MR, McNagny KM, Gold MR, Arrowsmith CH, Sato T, Rossi FMV, Tatlock JH, Owen DR, Brown PJ, Zaph C. SETD7 controls intestinal regeneration and tumorigenesis by regulating Wnt/β-catenin and Hippo/YAP signaling. Dev Cell 2016;37:47–57.
41. Miyoshi H, VanDussen KL, Malvin NP, Ryu SH, Wang Y, Sonnek NM, Lai C-W, Stappenbeck TS. Prostaglandin E2 promotes intestinal repair through an adaptive cellular response of the epithelium. EMBO J 2017;36:5–24.
42. Sprangers J, Zaalberg IC, Maurice MM. Organoid-based modeling of intestinal development, regeneration, and repair. Cell Death Differ 2021;28:95–107.
43. Mustata Roxana C, Vasile G, Fernandez-Vallone V, Strollo S, Lefort A, Libert F, Monteyne D, Pérez-Morga D, Vassart G, Garcia M-I. Identification of Lgr5-independent spheroid-generating progenitors of the mouse fetal intestinal epithelium. Cell Rep 2013;5:421–432.
44. Meriwether D. Novel Distinct Roles for Intestinal/Macrophage COX-2 and Apolipoprotein Mimetic Peptides in the Development and Treatment of Inflammatory Bowel Diseases. Dissertation. UCLA. https://escholarship.org/uc/item/0dz2d9wt. 2018. Accessed November 15, 2021.
45. Vieira SM, Lemos HP, Grespan R, Napimoga MH, Dal-Secco D, Freitas A, Cunha TM, Verri WA Jr, Souza-Junior DA, Jamur MC, Fernandes KS, Oliver C, Silva JS, Teixeira MM, Cunha FQ. A crucial role for TNF-alpha in mediating neutrophil influx induced by endogenously generated or exogenous chemokines, KC/CXCL1 and LIX/CXCL5. Br J Pharmacol 2009;158:779–789.
46. Fournier BM, Parkos CA. The role of neutrophils during intestinal inflammation. Mucosal Immunol 2012; 5:354–366.
47. Onali S, Favale A, Fantini MC. The resolution of intestinal inflammation: the peace-keeper's perspective. Cells 2019;8:344.
48. Morioka S, Maueröder C, Ravichandran KS. Living on the edge: efferocytosis at the interface of homeostasis and pathology. Immunity 2019;50:1149–1162.
49. Lee Chang S, Penberthy Kristen K, Wheeler Karen M, Juncadella Ignacio J, Vandenabeele P, Lysiak Jeffrey J, Ravichandran Kodi S. Boosting apoptotic cell clearance by colonic epithelial cells attenuates inflammation in vivo. Immunity 2016;44:807–820.
50. Dige A, Magnusson MK, Ohman L, Hvas CL, Kelsen J, Wick MJ, Agnholt J. Reduced numbers of mucosal DR(int) macrophages and increased numbers of CD103(+) dendritic cells during anti-TNF-alpha treatment in patients with Crohn's disease. Scand J Gastroenterol 2016;51:692–699.
51. Ruder B, Becker C. At the Forefront of the mucosal barrier: the role of macrophages in the intestine. Cells 2020;9:2162.
52. Nakanishi Y, Nakatsuji M, Seno H, Ishizu S, Akitake-Kawano R, Kanda K, Ueo T, Komekado H, Kawada M, Minami M, Chiba T. COX-2 inhibition alters the phenotype of tumor-associated macrophages from M2 to M1 in ApcMin/+ mouse polyps. Carcinogenesis 2011; 32:1333–1339.
53. Tang T, Scambler TE, Smallie T, Cunliffe HE, Ross EA, Rosner DR, O'Neil JD, Clark AR. Macrophage responses to lipopolysaccharide are modulated by a feedback loop involving prostaglandin E2, dual specificity phosphatase 1 and tristetraprolin. Sci Rep 2017;7:4350.
54. Wang X, Yao B, Wang Y, Fan X, Wang S, Niu A, Yang H, Fogo A, Zhang MZ, Harris RC. Macrophage cyclooxygenase-2 protects against development of diabetic nephropathy. Diabetes 2017;66:494–504.
55. Yang R, Chiang N, Oh SF, Serhan CN. Metabolomics-lipidomics of eicosanoids and docosanoids generated by phagocytes. Curr Protoc Immunol 2011;Chapter 14: Unit 14 26.
56. Yoon Y-S, Lee Y-J, Choi Y-H, Park YM, Kang JL. Macrophages programmed by apoptotic cells inhibit epithelial-mesenchymal transition in lung alveolar epithelial cells via PGE2, PGD2, and HGF. Sci Rep 2016; 6:20992.
57. Cai B, Thorp EB, Doran AC, Subramanian M, Sansbury BE, Lin C-S, Spite M, Fredman G, Tabas I. MerTK cleavage limits proresolving mediator biosynthesis and exacerbates tissue inflammation. Proc Natl Acad Sci U S A 2016;113:6526.
58. Cai B, Kasikara C, Doran AC, Ramakrishnan R, Birge RB, Tabas I. MerTK signaling in macrophages promotes the synthesis of inflammation resolution mediators by suppressing CaMKII activity. Sci Signal 2018; 11:eaar3721.
59. Fadok VA, Bratton DL, Konowal A, Freed PW, Westcott JY, Henson PM. Macrophages that have ingested apoptotic cells in vitro inhibit proinflammatory cytokine production through autocrine/paracrine mechanisms involving TGF-beta, PGE2, and PAF. J Clin Invest 1998;101:890–898.
60. Norris PC, Dennis EA. A lipidomic perspective on inflammatory macrophage eicosanoid signaling. Adv Biol Regul 2014;54:99–110.
61. Sorgi CA, Zarini S, Martin SA, Sanchez RL, Scandiuzzi RF, Gijón MA, Guijas C, Flamand N, Murphy RC, Faccioli LH. Dormant 5-lipoxygenase in inflammatory macrophages is triggered by exogenous arachidonic acid. Sci Rep 2017;7:10981.

62. Chinen T, Komai K, Muto G, Morita R, Inoue N, Yoshida H, Sekiya T, Yoshida R, Nakamura K, Takayanagi R, Yoshimura A. Prostaglandin E2 and SOCS1 have a role in intestinal immune tolerance. Nat Commun 2011;2:190.
63. Kong D, Shen Y, Liu G, Zuo S, Ji Y, Lu A, Nakamura M, Lazarus M, Stratakis CA, Breyer RM, Yu Y. PKA regulatory IIalpha subunit is essential for PGD2-mediated resolution of inflammation. J Exp Med 2016; 213:2209–2226.
64. Kim W, Lee HN, Jang JH, Kim SH, Lee YH, Hahn YI, Ngo HK, Choi Y, Joe Y, Chung HT, Chen Y, Cha YN, Surh YJ. 15-Deoxy-Δ(12,14)-prostaglandin J(2) exerts proresolving effects through nuclear factor E2-related factor 2-induced expression of CD36 and heme oxygenase-1. Antioxid Redox Signal 2017;27:1412–1431.
65. van der Flier LG, Clevers H. Stem cells, self-renewal, and differentiation in the intestinal epithelium. Annu Rev Physiol 2009;71:241–260.
66. Clevers H. The intestinal crypt, a prototype stem cell compartment. Cell 2013;154:274–284.
67. Lacy ER. Epithelial restitution in the gastrointestinal tract. J Clin Gastroenterol 1988;10(Suppl 1):S72–S77.
68. Stappenbeck TS, Miyoshi H. The role of stromal stem cells in tissue regeneration and wound repair. Science 2009;324:1666–1669.
69. Blikslager AT, Moeser AJ, Gookin JL, Jones SL, Odle J. Restoration of barrier function in injured intestinal mucosa. Physiol Rev 2007;87:545–564.
70. Iizuka M, Konno S. Wound healing of intestinal epithelial cells. World J Gastroenterol 2011;17:2161–2171.
71. Seno H, Miyoshi H, Brown SL, Geske MJ, Colonna M, Stappenbeck TS. Efficient colonic mucosal wound repair requires Trem2 signaling. Proc Natl Acad Sci U S A 2009; 106:256–261.
72. Watanabe J, Lin JA, Narasimha AJ, Shahbazian A, Ishikawa T-o, Martin MG, Herschman HR, Reddy ST. Novel anti-inflammatory functions for endothelial and myeloid cyclooxygenase-2 in a new mouse model of Crohn's disease. Am J Physiol Gastrointest Liver Physiol 2010;298:G842–G850.
73. Reis MB, Pereira PAT, Caetano GF, Leite MN, Galvão AF, Paula-Silva FWG, Frade MAC, Faccioli LH. Lipoxin A4 encapsulated in PLGA microparticles accelerates wound healing of skin ulcers. PLoS One 2017;12:e0182381.
74. Narasimha AJ, Watanabe J, Ishikawa TO, Priceman SJ, Wu L, Herschman HR, Reddy ST. Absence of myeloid COX-2 attenuates acute inflammation but does not influence development of atherosclerosis in apolipoprotein E null mice. Arterioscler Thromb Vasc Biol 2010;30:260–268.
75. Sato T, Vries RG, Snippert HJ, van de Wetering M, Barker N, Stange DE, van Es JH, Abo A, Kujala P, Peters PJ, Clevers H. Single Lgr5 stem cells build crypt-villus structures in vitro without a mesenchymal niche. Nature 2009;459:262–265.
76. Wang B, Rong X, Palladino END, Wang J, Fogelman AM, Martín MG, Alrefai WA, Ford DA, Tontonoz P. Phospholipid remodeling and cholesterol availability regulate intestinal stemness and tumorigenesis. Cell Stem Cell 2018;22:206–220.e4.
77. Metsalu T, Vilo J. ClustVis: a web tool for visualizing clustering of multivariate data using principal component analysis and heatmap. Nucleic Acids Res 2015; 43:W566–W570.

Received March 22, 2021. Accepted January 3, 2022.

Correspondence
Address correspondence to: David Meriwether, PhD, Department of Medicine, Division of Digestive Diseases, David Geffen School of Medicine at UCLA, University of California Los Angeles, 10833 Le Conte Avenue, Los Angeles, CA 90095-5347. e-mail: dmeriwether@mednet.ucla.edu; fax: 310-206-3605. or Srinivasa T. Reddy, PhD, Department of Medicine, David Geffen School of Medicine at UCLA, 10833 Le Conte Avenue, Room 43-144 CHS, Los Angeles, CA 90095-1679. e-mail: sreddy@mednet.ucla.edu; fax: 310-206-3605.

Conflicts of interest
These authors disclose the following: Alan M. Fogelman and Srinivasa T. Reddy are principals in Bruin Pharma, and Alan M. Fogelman is an officer in Bruin Pharma. The remaining authors disclose no conflicts.

Funding
This work was supported in part by U.S. Public Health Service Research Grant Nos. R01 HL148286 (to Alan M. Fogelman) and R01 HL129051 (to Srinivasa T. Reddy), and the Laubisch, Castera, and M.K. Grey Funds at the University of California, Los Angeles. This work was further supported by grants from the National Institute of Diabetes and Digestive and Kidney Diseases (Nos. DK085535, DK41301, and DK118640 [to Martin G. Martin]). Further support was provided by National Institutes of Health Grant Nos. R35 GM138003 and P30 DK063491 (to Ajit S. Divakaruni). Anthony E. Jones was supported by UCLA Tumor Cell Biology Training Grant No. T32 CA009056. Julia J. Mack was supported by the American Heart Association Award No. 19CDA34760007.